6/13-96 JS (1)

SANDIA REPORT

SAND96–2739 • UC–906
Unlimited Release
Printed November 1996

High-Frequency Scannerless Imaging Laser Radar for Industrial Inspection and Measurement Applications

R. L. Schmitt, R. J. Williams, J. D. Matthews

Prepared by
Sandia National Laboratories
Albuquerque, New Mexico 87185 and Livermore, California 94550
for the United States Department of Energy
under Contract DE-AC04-94AL85000

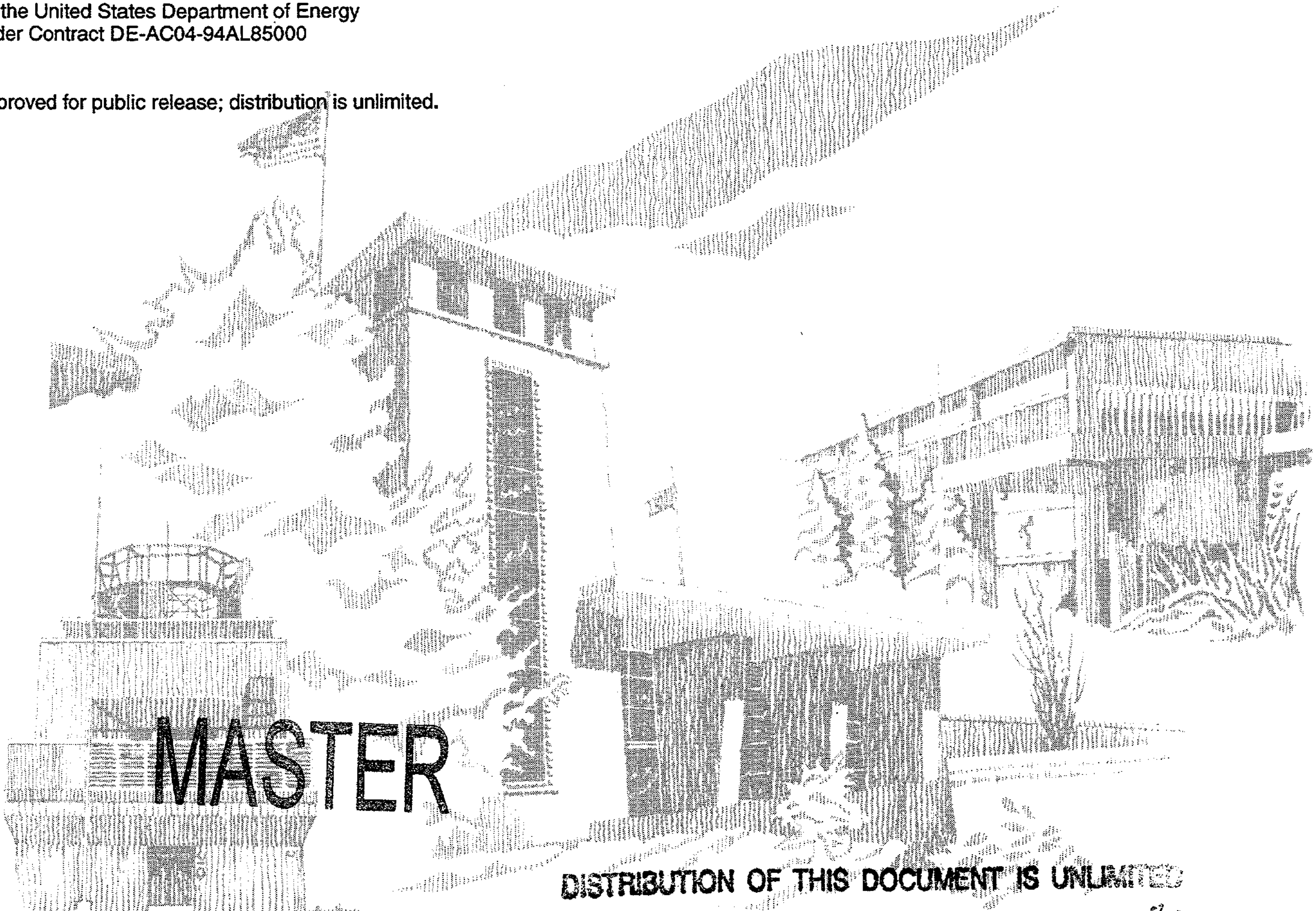

MASTER

DISTRIBUTION OF THIS DOCUMENT IS UNLIMITED

2

Issued by Sandia National Laboratories, operated for the United States Department of Energy by Sandia Corporation.

Printed in the United States of America. This report has been reproduced directly from the best available copy.

Available to DOE and DOE contractors from
Office of Scientific and Technical Information
PO Box 62
Oak Ridge, TN 37831

Prices available from (615) 576-8401, FTS 626-8401

Available to the public from
National Technical Information Service
US Department of Commerce
5285 Port Royal Rd
Springfield, VA 22161

NTIS price codes
Printed copy: A04
Microfiche copy: A01

SAND96-2739
Unlimited Release
Printed November 1996

Distribution
Category UC-906

High-frequency scannerless imaging laser radar for industrial inspection and measurement applications

R. L. Schmitt
Laser, Optics, and Remote Sensing Department

R. J. Williams
Frequency and Optoelectronics Applications Department

J. D. Matthews
Firing Set and Contact Fuze Department

Sandia National Laboratories
Albuquerque, NM 87185-1423

Abstract

This report describes the development and testing of a high-frequency scannerless imaging laser radar system to evaluate its viability as an industrial inspection and measurement sensor. We modified an existing 5.5-Mhz scannerless laser radar to operate at 150 Mhz, and measured its performance including its spatial resolution and range resolution. We also developed new algorithms that allow rapid data reduction with improved range resolution. The resulting 150-Mhz ladar system demonstrated a range resolution of better than 3 mm, which represents nearly a factor-of-100 improvement in range resolution over the existing scannerless laser radar system. Based on this work, we believe that a scannerless range imager with 1- to 2-mm range resolution is feasible. This work was performed as part of a small-business CRADA between Sandia National Laboratories and Perceptron, Inc.

Contents

Figures

High-frequency scannerless laser radar for industrial inspection and measurement applications.

Introduction

Three-dimensional measurement and inspection of parts during manufacturing is a key element in modern manufacturing. Data gathered by these inspections is not simply used as criteria to reject out-of-tolerance parts, but rather, as feedback to the manufacturing process itself, allowing fine adjustment of the machines that produce the parts. Inspection of automobile body panels, for example, requires measurement of not only the shape of the part, but the precise location of fastener holes and other interface features to ensure that the final assembly will fit together properly. In the end, the goodness-of-fit of an automobile body affects not only the appearance of the vehicle, but the rattles, vibration, and wind noise that the occupants experience as the car is driven. Since timely feedback in these complex manufacturing processes is crucial, the data collection rate, ease of use, and flexibility to measure a variety of different parts are all important aspects of any useful industrial inspection device.

Current inspection technology used in automobile manufacturing frequently employs a variety of optical triangulation gauges mounted on a test stand to measure tens of fiducial locations on each part. Since each triangulation gauge only measures a single point, or, at most, points along a line, the test stand for typical part such as an automobile fender, requires many individual gauges and a rather laborious setup, alignment, and calibration of these gauges that is unique to each part. Thus, a separate measurement stand is needed for each part, and the setup of each stand is very time consuming. A three-dimensional imaging sensor, such as an imaging laser radar, on the other hand, could produce a three-dimensional map of the part over a relatively wide area, and, as a result, would be a much more flexible inspection sensor. With an imaging laser radar, any number of fiducials within the sensor's field-of-view could be measured simultaneously. If the size of the part exceeded the field-of-view of the ladar, the sensor could be mechanically scanned across the part or several sensors could be employed to view the entire part at once. In either case, the time required to setup, align, and calibrate the sensor for a new part would be drastically reduced from the time required to set up numerous triangulation gauges.

It is the need for flexible, easy-to-use, three-dimensional inspection sensors for manufacturing that motivates this work. Although several scanning laser radars are commercially available, these devices are not ideally suited for the manufacturing environment. Their principal drawback is the fact that the 3-D image data is acquired serially by raster scanning a narrow laser beam across the desired field of view. The serial nature of the data acquisition for these scanning sensors severely limits their data rate, and the opto-mechanical scanners used are generally very expensive, physically large, delicate (sensitive to shock and vibration), and require periodic maintenance for reliable operation. Sandia has developed a scannerless imaging laser radar[1-3] which overcomes the limitations imposed by scanning systems. (Readers who are not familiar with laser radar may refer to Appendix A which gives an overview and theory of scannerless laser radar.) Our scannerless range imaging technique eliminates the need for a mechanical laser beam scanner to illuminate and readout the scene, and, as a result, allows higher data rates, and increased compactness and ruggedness of the sensor.

The overall goal of this CRADA project was to determine the suitability of the scannerless laser radar for measurement and inspection applications in industrial manufacturing (for example, automobile manufacturing). Specifically, we were interested in determining whether or not the spatial and range resolution of the scannerless ladar could be made small enough to be of practical value for industrial inspection. To accomplish this, we modified an existing scannerless range imaging system to provide an appropriate field of view and increased range resolution. We then tested the modified ladar to measure its spatial resolution and range resolution. The main emphasis of this report is to describe the hardware modifications to the ladar, the data that was collected with the modified ladar, and the analysis of the data to measure the performance of the ladar. We have described the details of the theory of scannerless laser radar in Appendix A, and the details of the algorithms we use to convert the raw data into range images in Appendix B.

Overview of Scannerless Laser Radar

The theory of the scannerless laser radar is described in detail in Appendix A, but we will review the basic concepts here. A schematic diagram of the scannerless ladar is shown in Figure 1. An optical source (typically a laser diode) is intensity modulated at some frequency, f_m, and used to illuminate the entire field of view of the scene of interest. A lens collects light scattered from the scene and images it onto an image intensifier tube. Light collected from the scene experiences a round-trip phase shift relative to the transmitted light, ϕ,and this phase shift is proportional to the distance to the scene. The range to the target pixel is given by the cw ladar equation:

$$R = \frac{c\phi}{4\pi f_m} \qquad (1)$$

where c is the speed of light. The phase shift to the target pixel (and thereby the range to each pixel in the scene) is measured by modulating the gain of the image intensifier tube at the same frequency and synchronously with the illumination source, and then integrating and storing the output of the image intensifier on a charge coupled device (CCD) camera. The resultant image contains information about the phase shift to each pixel in the scene. Thus, the scannerless laser radar is a phase-sensitive imaging device in which each pixel of the CCD contains information to determine the range to each corresponding point in the scene.

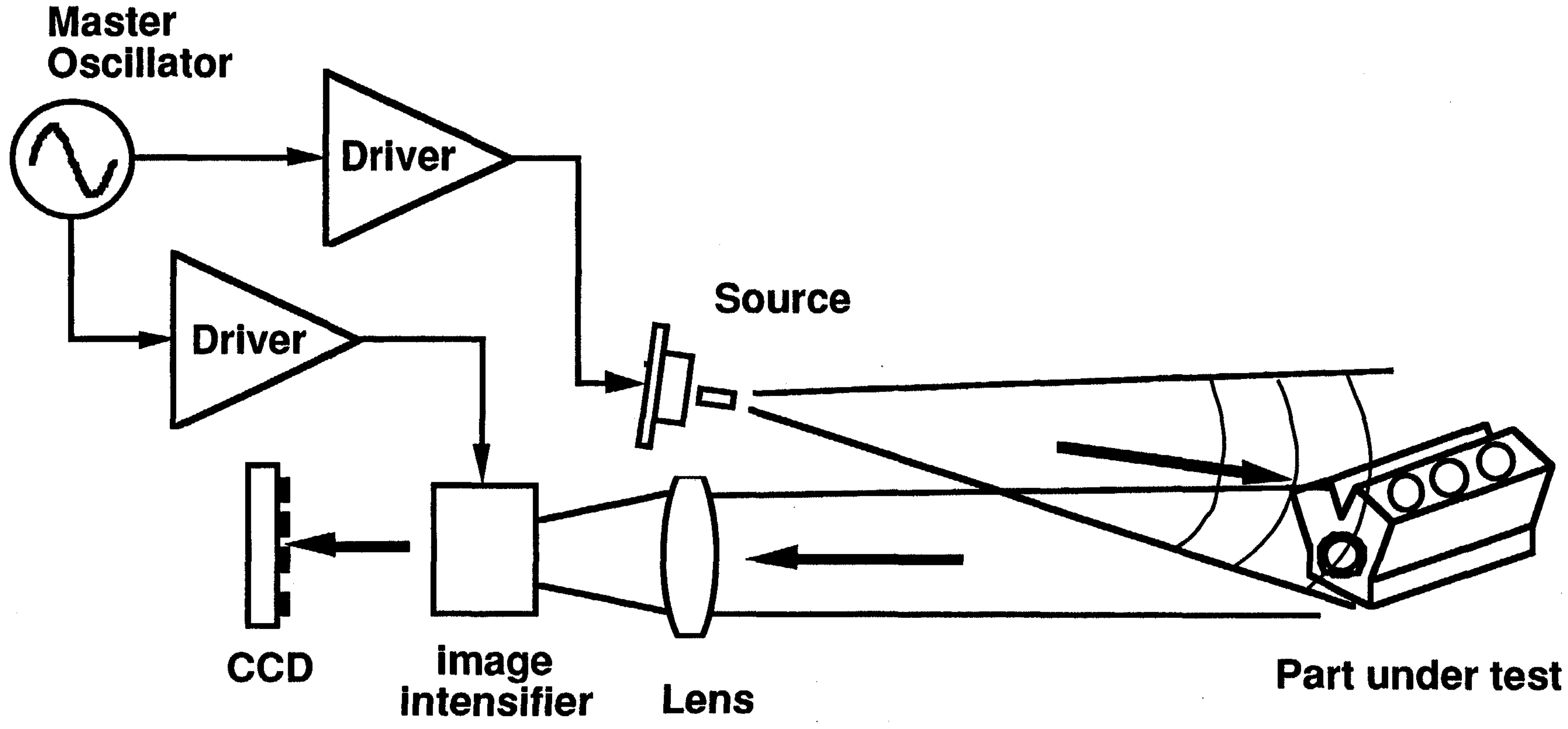

Figure 1. Schematic diagram of scannerless imaging laser radar. The part under test is broadly illuminated with a sinusoidal intensity-modulated laser beam. Light scattered from the part is collected by a lens and imaged onto an image intensifier tube. The gain of the image intensifier tube is modulated at the same frequency and synchronously with the illumination laser and its output is integrated and recorded on a two-dimensional CCD array. The entire system is a phase-sensitive imaging system that can measure the distance to each point in its field of view.

Sandia's scannerless laser radar was originally developed for defense applications such as physical security and surveillance systems which typically require fields of view ~10 m by 30 m wide at distances of ~100 m or more with spatial and range resolution of ~0.3 m. Industrial inspection applications, on the other hand, require a rather small field of view (~1 m by 1 m) with much finer range resolution (~1 mm or better). While the field of view of the scannerless ladar can be changed simply by changing the focal length of the lens used to image the scene, the range resolution depends on the modulation frequency and the signal-to-noise ratio (SNR) of the data. An approximate relationship for the range resolution, ΔR, of a cw laser radar is given by:

$$\Delta R = \frac{c}{4\pi f_m \sqrt{2}\, SNR} \qquad (2)$$

where SNR is the signal-to-noise ratio of the measurement. Thus, the only ways to improve the range resolution are to either increase the modulation frequency f_m, and/or increase the SNR.

In order to increase the range resolution of our existing 5.5-Mhz ladar, we chose to increase the operating frequency, f_m, and to improve the SNR by collecting more data and using new data processing algorithms to convert the raw data into range images. Since the existing 5.5-Mhz ladar had a range resolution of approximately 0.3 m, a modulation frequency in excess of 1.6 Ghz would be required to achieve our goal of ~1 mm range resolution with simply a change in modulation frequency. Although image intensifier tubes have been modulated at frequencies greater than 1 Ghz for non-imaging applications, we were not confident that the image quality could be preserved at such high modulation frequencies. Instead, we chose to attempt to modulate the image intensifier at frequencies between 100 Mhz and 500 Mhz, and achieve the balance of the range resolution improvement from improvements in the SNR of the data and the algorithms for processing the raw data into range images.

Electronic Drive Circuit Modifications

The requirements for the new electronic drive circuits were twofold: First, the system must be able to drive both a laser diode and the image intensifier gain at frequencies as high as possible. Our goal was to operate the system somewhere between 100 Mhz and 500 Mhz. Second, the system must allow a variable phase shift to be inserted between the image intensifier and the laser diode. This requirement facilitates the new data collection/processing based on phase-shifting interferometry (described in detail in Appendix B).

Due to both time and budgetary pressures, we chose to drive the electronic system using two Hewlett-Packard 3335A frequency synthesizers. These signal generators operate at frequencies up to 80 Mhz and allow programmable phase shifts either through their front-panel controls or through IEEE-488 (GPIB) interfaces. The IEEE-488 interface was a very convenient interface to the existing instrument control and data collection software for the ladar. In order to extend the frequency range of these signal generators, we built external circuitry to frequency double the output. Thus, we were able to modulate the image intensifier tube and the laser diode at frequencies up to 160 Mhz with computer-controlled variable phase shift between the transmitter (laser) and receiver (image intensifier).

A schematic of the data acquisition system is shown in Figure 2. The system is built around a standard Intel-based personal computer using an ISA bus for all of the interfaces. A 486 CPU and its associated memory, disk space, and video display form the platform from which the data acquisition software is developed and executed. An IEEE-488 interface allows the system to communicate with and control the two H/P frequency synthesizers as well as other peripherals as needed. A digital I/O board sends commands to custom circuitry that controls the CCD camera timing. The CCD camera is a Dalsa 256 x 256 array with an onboard 8-bit analog-to-digital converter (ADC). The 8-bit video data from the CCD camera is sent directly to an Alacron digital signal processing (DSP) board which stores the raw data and is capable of processing the raw data into range images. The Alacron uses its own i860 CPU and 16 Mbytes of onboard memory for data storage and processing, and produces its own display of the data on a video monitor.

A more detailed schematic of the electronics used to drive the laser and the image intensifier tube (circuits developed specifically for this project) is shown in Figure 3. The master oscillator output of one of the synthesizers was tied to the master oscillator input of the other to ensure that both operated at the same frequency and that the phase relationship between the two was stable. The relative phase shift between the two synthesizers was controlled by the data acquisition computer through the IEEE-488 interface. The outputs from each of the synthesizers were frequency doubled in external circuits using AD835 4-quadrant analog signal multipliers. One of the frequency-doubled synthesizers directly modulated the laser diode (Spectra Diode Labs model 5430-G1) used to illuminate the scene. A variable DC bias was applied to the laser to operate it at the desired average output while the sinusoidal signal from the synthesizer modulated the light output about the average value. The other frequency-doubled synthesizer was sent to an ENI model 325 RF power amplifier which then drove the photocathode of the image intensifier to modulate its gain. A variable DC bias was used to set the average gain of the intensifier.

Experimental Setup

The optical setup of the ladar receiver used for this project is shown in Figure 4. A lens imaged the scene onto the photocathode of the image intensifier tube. For most of the experiments described here, the lens was a 75-mm-focal-length CCTV lens. The output phosphor of the image intensifier was coupled to the fiber-optic faceplate of the CCD using a 3:1 imaging-fiber-optic taper. Thus, the 18-mm-

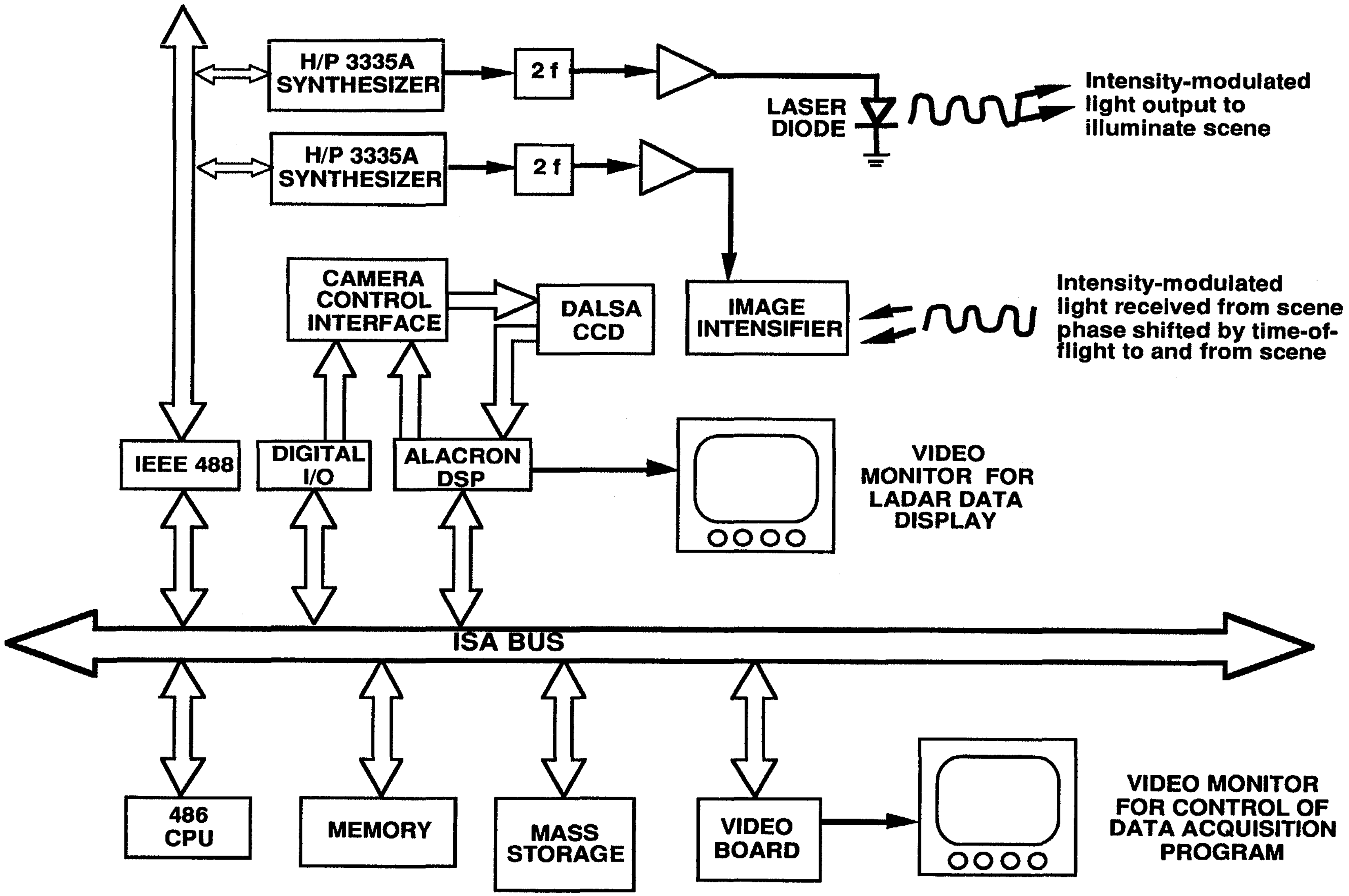

Figure 2. Schematic diagram of the scannerless laser radar data acquisition system.

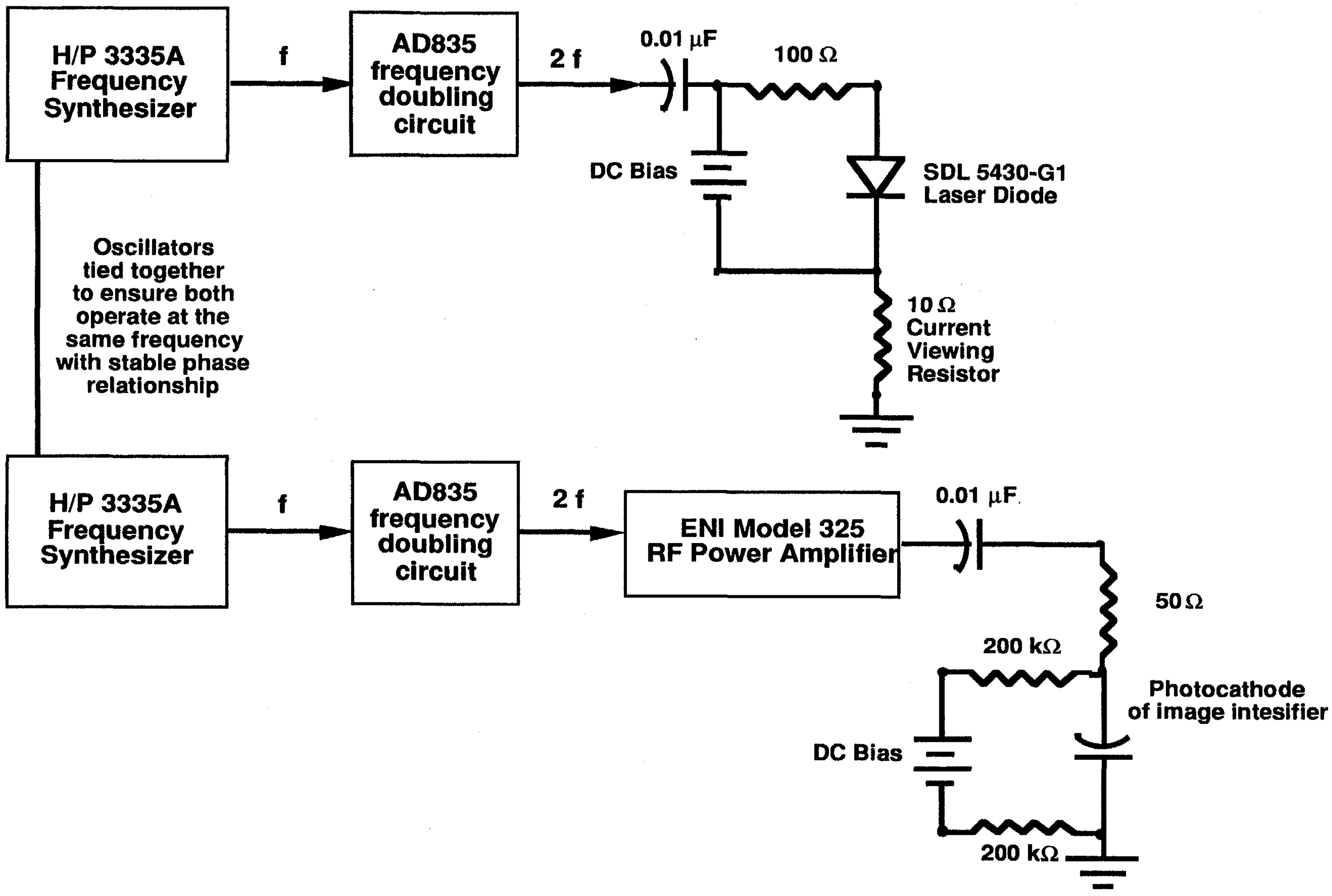

Figure 3. Schematic diagram of the electronic drive system for the transmitter and receiver.

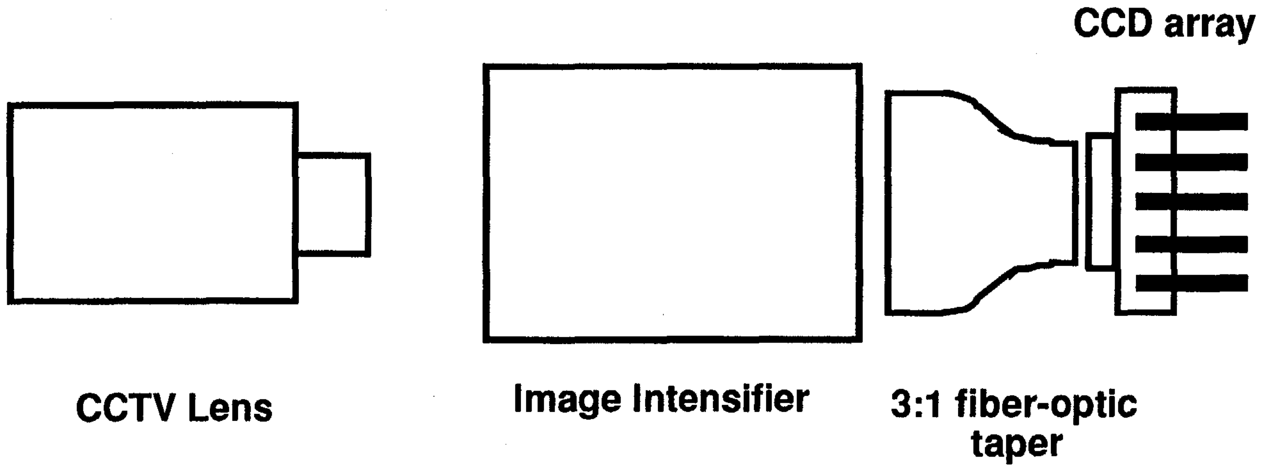

Figure 4. Optical train for the scannerless laser radar receiver. A CCTV lens is used to image the scene onto the photocathode of an image intensifier tube. The output phosphor of the image intensifier is coupled to the CCD array with a 3:1 fiber-optic taper that matches the image size on the phosphor to the size of the CCD.

diameter photocathode was well matched to the ~6 x 6-mm CCD chip. Optical index matching fluid was used between all fiber-optic interfaces to ensure low transmission loss and good spatial resolution. In spite of the great care taken to optimize the coupling between the image intensifier and the CCD, the components did shift slightly after assembly, and this caused a slight separation between the fiber bundle and the CCD on one corner. As a result, the spatial resolution of the data acquired with this system was not optimal, particularly on one edge and two corners of the image (as we will show later).

The general arrangement of scannerless ladar experiments is shown in Figure 5. A flat panel located 1.33 m from the ladar receiver served as a background for all of the experiments. It was positioned normal to the optical centerline of the receiver and was large enough in area to completely fill the field of view of the receiver. The laser illuminator was placed as close as possible to the lens of the ladar receiver to minimize the parallax between the transmitted and returned light. Various targets, such as the movable flat panel shown in the figure, were positioned in front of the flat background.

Data Collection and Processing

The data collection and processing for this project differs markedly from our previous methods. In an effort to obtain the highest possible signal-to-noise in the range images we chose to adapt data collection methods and data fitting algorithms that have been successfully used in the field of phase-stepping interferometry for many years. The details of the algorithms are given in Appendix B and references contained therein. Briefly, we collect N images of the scene of interest. Each image is collected using a different relative phase shift, δ, between the transmitter and receiver. Normally, these phase shifts are uniformly spaced over the interval 0 to 2π, but this is not a requirement. The intensity at each pixel of each image must satisfy the equation:

$$I = A + B\cos(\phi + \delta) \qquad (3)$$

where ϕ is the phase shift due to the range to the object pixel, A is the average intensity at each pixel, and B is the depth of modulation at each pixel. If we use the N images and the known phase shifts δ_i as input to a least squares fitting routine we can determine ϕ, A and B for each pixel in the scene.

Note that equation (3) assumes that the transmitter and receiver are linear. In fact, the gain of the image intensifier tube is a nonlinear function of the drive voltage, and other components in the system also deviate from linearity. In spite of these nonlinearities, we have found that equation 3 fits the data well. It is beyond the scope of this project to evaluate the effects of nonlinearities in the system, but one expects nonlinearities to generate harmonics of the ladar operating frequency in the recorded signal, and these harmonics may affect the range images slightly.

TOP VIEW

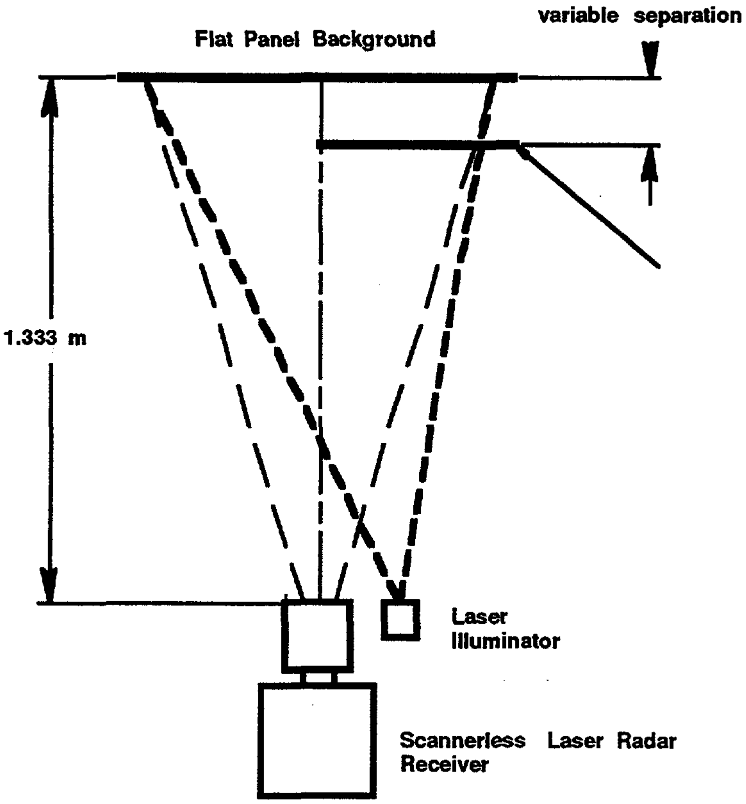

Figure 5 Basic data collection geometry for range resolution measurements.

Our previous data collection and reduction techniques relied on collecting three frames of raw data: Two frames corresponding to $\delta = 0$ and $\delta = \pi / 2$ relative phase shift and one frame which was a simple reflectivity image of the scene used to normalize the data for $1 / R^2$, illumination nonuniformity, and target albedo variations. The signal-to-noise ratio (and thus the range resolution) of the range images produced from this 3-frame technique is limited due to the SNR of the individual frames of data. The new N-frame technique, on the other hand, allows an improvement in SNR which should approach $\sqrt{N}$, thereby allowing us to improve range resolution at the expense of the additional time required to acquire and process the data.

The sequence of N input images is obtained by setting the relative phase shift between the transmitter and receiver (using the IEEE-488 interface to the synthesizers) to a starting value (usually 0) and acquiring one frame of video data from the CCD. Then the phase shift is incremented, and another frame of data is collected. After the process has been repeated N times, the N frames of data are written to disk for storage and off-line analysis. For this project, we chose to use the Alacron DSP only as a video frame acquisition and storage device and perform all data analysis off-line, although in an operational system the DSP could perform the data reduction in real-time. By storing the all of the raw data, we are free to analyze the data many times in a variety of different ways to determine not only the best algorithms to use, but also the optimal number of raw data frames to collect for our range images.

Overview of the Experimental Test Plan

The principal objectives of this work were to measure the spatial resolution and range resolution of the scannerless laser radar operating at high modulation frequency. Also of interest were investigating the interaction between the spatial resolution and range resolution, and the development of data collection schemes and data processing algorithms that improve the performance of the ladar system. The following sections describe the experiments we performed, show the data we obtained, and discuss the analysis of the data.

Spatial Resolution

Spatial resolution is a measure of how well an optical system can distinguish between two separate features in a scene. There are many definitions of spatial resolution in use in the optical field, and these definitions vary depending on the specific optical system and its end-use application. Defining a metric for spatial resolution can be especially tricky when a human observers are involved in the interpretation and evaluation of the images, since the image with the best resolution may not look the best to a human observer[4].

Perhaps the most straightforward way to define and then measure the spatial resolution for the scannerless laser radar is to use the concepts of optical transfer function (OTF) and modulation transfer function (MTF). The optical transfer function is a mathematical way of describing the spatial frequency response of an optical system. (The theory and application of OTF is described in a number of texts on Fourier optics[4-6].) It can be measured by imaging targets with known spatial frequency content (usually black and white bar targets) and comparing the optical system response to the input. The most common target in use is the USAF standard resolution target which contains sets of black on white (or chrome on clear glass) bars with various spacing (spatial frequencies) and orientations. Another target, which we have chosen to use for this project, is a simple edge target consisting of a very wide black bar on a white background. This test object is a step function which contains all spatial frequencies. The frequency response of the optical system is measured by analyzing the transition from black to white. This so-called edge response of the optical system can be directly related to the optical transfer function and used as a metric for comparison of the spatial resolution of the system.

The experimental arrangement and target used for measuring the spatial resolution of the scannerless laser radar are shown in Figure 6. The ladar transmitter and receiver are located ~1.3 m from a flat target plane (the same background target used for all of the range resolution measurements). The target was covered with auto-primer-gray paint to provide a uniform-albedo target. An L-shaped black target was placed on the background to provide a step function for both the horizontal and vertical dimensions. Typical image data from this target is shown in Figure 7. Note that the left edge and left-hand corners of the field of view are black due to poor optical coupling between the image-intensifier tube/fiber taper/CCD fiber plate interfaces. Unfortunately, the mechanical hardware used to hold the intensified CCD (ICCD) was not able to fully compensate for small wedge angles of the mating optical surfaces with respect to housings of these components. Despite our best efforts, we were not able to achieve optimal coupling between the ICCD components and chose to spend the rest of our time for this project refining the high-frequency modulation and data reduction techniques instead of optimizing the spatial resolution. Future systems will be designed fix this problem and achieve the optimal resolution of the intensified CCD camera system.

A horizontal cut through the image data is plotted in Figure 7-b. Note that the light and dark regions are not constant in intensity due to the non-uniform illumination pattern of the laser diode. Also, the transition from light to dark is not extremely sharp, due to blurring by the ICCD optical system. It is the sharpness of this transition that we analyze to determine the spatial resolution of the system.

The data presented in Figure 7-b is called the edge response of the optical system. Mathematically, it is the convolution of a step function (the sharp light to dark transition of the target) with the line spread function of the optical system. The edge response is also the integral of the line spread function, allowing us to simply differentiate the image data we have collected to yield the line spread function of

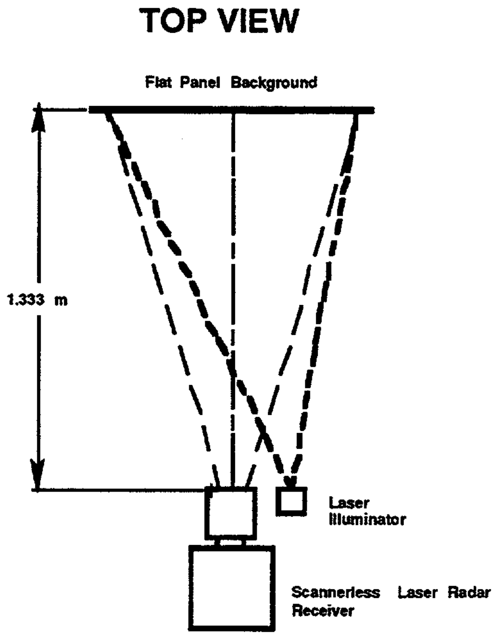

(a) Optical setup for spatial resolution measurements

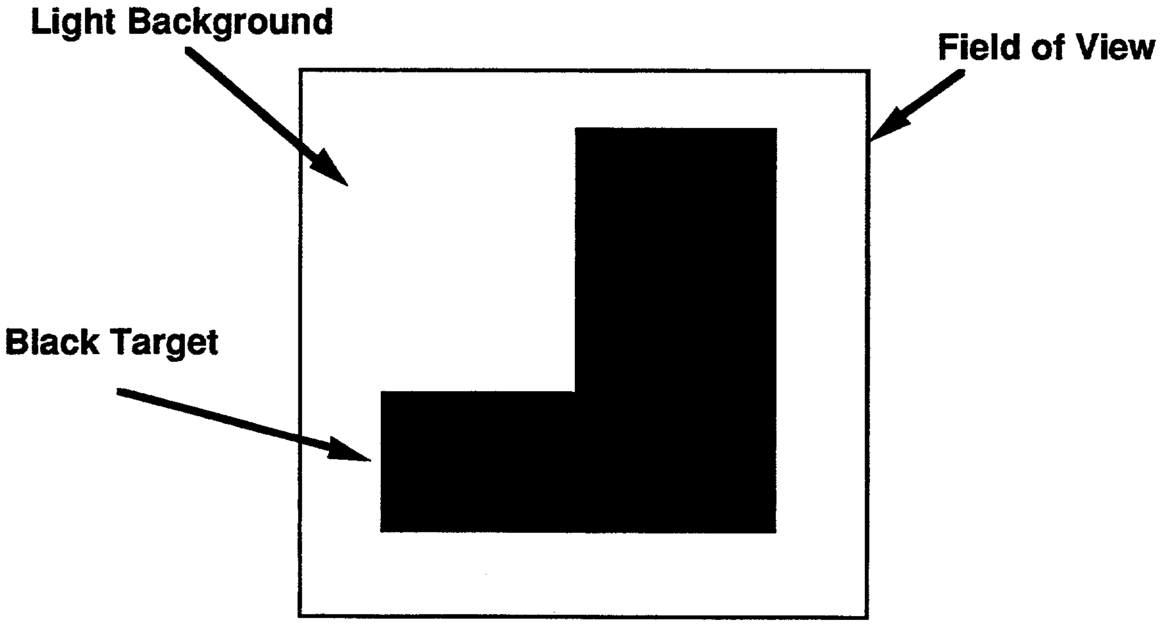

(b) Target used to measure spatial resolution

Figure 6. Setup for spatial resolution measurement including target.

(a) intensity stretched image

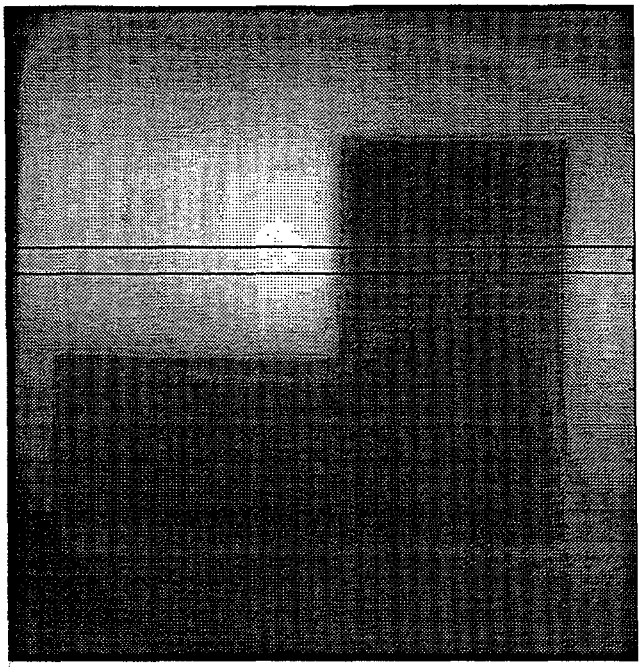

(b) horizontal profile centered at y=100 11 lines wide

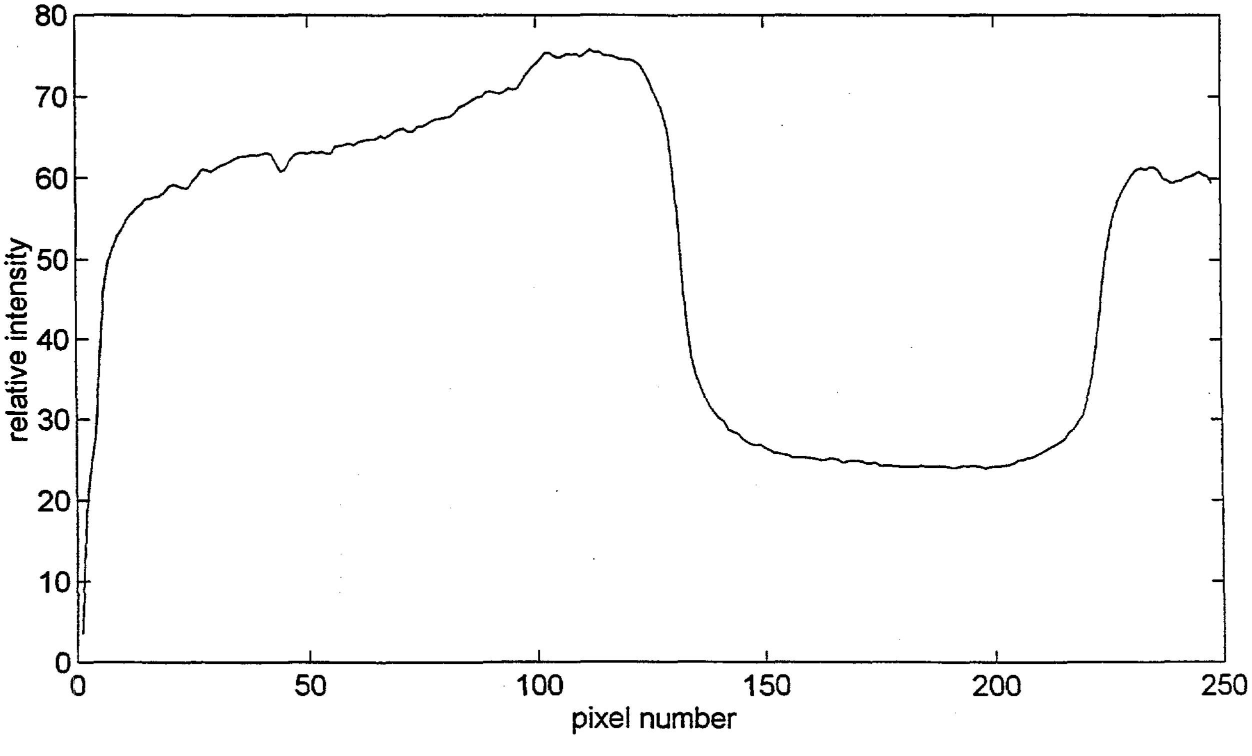

Figure 7. Data from the spatial resolution measurement.

our system. The Fourier transform of the line spread function is the optical transfer function[4-6]. Finally, the real part of the OTF is the MTF, the quantity of interest for our metric of spatial resolution. The transformation of our measured image data to MTF is illustrated in Figure 8. First, we selected a subset of the original data that included the light-to-dark transition and enough data on both sides of the transition to define the light and dark levels well. Data that exhibited the known intensity variation due to the non-uniform illumination and did not contribute information about the light-to-dark transition was cropped. A plot of the data that we selected for further processing is shown in Figure 8-a. Next, to facilitate the Fourier transform process, we added data points on both ends of the scan with intensity set equal to the mean light and dark levels respectively. This new data set, shown in Figure 8-b, was then differentiated to produce the line spread function shown in Figure 8-c. Finally, the line spread function was Fourier transformed to produce the optical transfer function. The real part of the OTF, the MTF, is plotted in Figure 8-d. The spatial frequency axis in Figure 8-d is scaled using the known pixel-to-pixel spacing of the CCD in the plane of the phosphor of the image intensifier tube. Since the CCD pixels are spaced on 16-μm centers and a 3:1 fiber taper images these pixels onto the image intensifier output plane, the Nyquist frequency for the ICCD is

$$f_{Nyquist} = \frac{1}{2 \bullet 3 \bullet 16 \bullet 10^{-3} mm} = 10.4\, lpm$$

The measurement of the MTF of our system indicates a cutoff frequency (MTF<5%) of ~5 lpm, a somewhat disappointing value since the Nyquist frequency for the CCD is 10 lpm and the cutoff frequency for the image intensifier tube is nearly 20 lpm.

To get a better idea of how our current optical system is performing relative to an optimally coupled system, we modeled the MTF of entire ICCD system. Using established models[7] for the individual components in the system we modeled the contribution to the overall MTF from the following ICCD components:

- image transfer from the photocathode to the MCP (this is a function of the photocathode-to-MCP voltage)
- image transfer through the MCP
- image transfer from the MCP to the output phosphor (this is a function of the MCP-to-phosphor voltage)
- image blurring due to the phosphor itself
- image blurring due to the fiber-optic faceplate interfaces (2 interfaces were considered assuming optimal coupling between these interfaces)

The contributions to the ICCD MTF from the CCD and the image intensifier are shown in Figure 9. The MTF of the image intensifier is a function of the photocathode-to-MCP voltage[7] (among other parameters), and we have plotted the overall ICCD MTF for various values of photocathode-to-MCP voltage ranging from 180 V to 10 V. This range corresponds to the maximum recommended

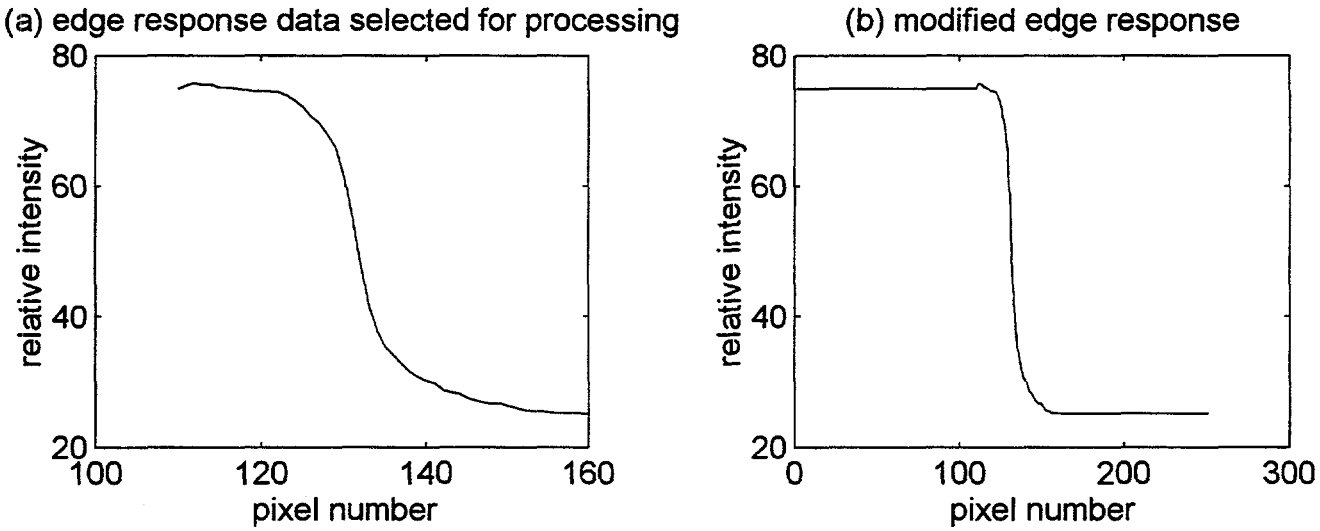

(a) edge response data selected for processing

(b) modified edge response

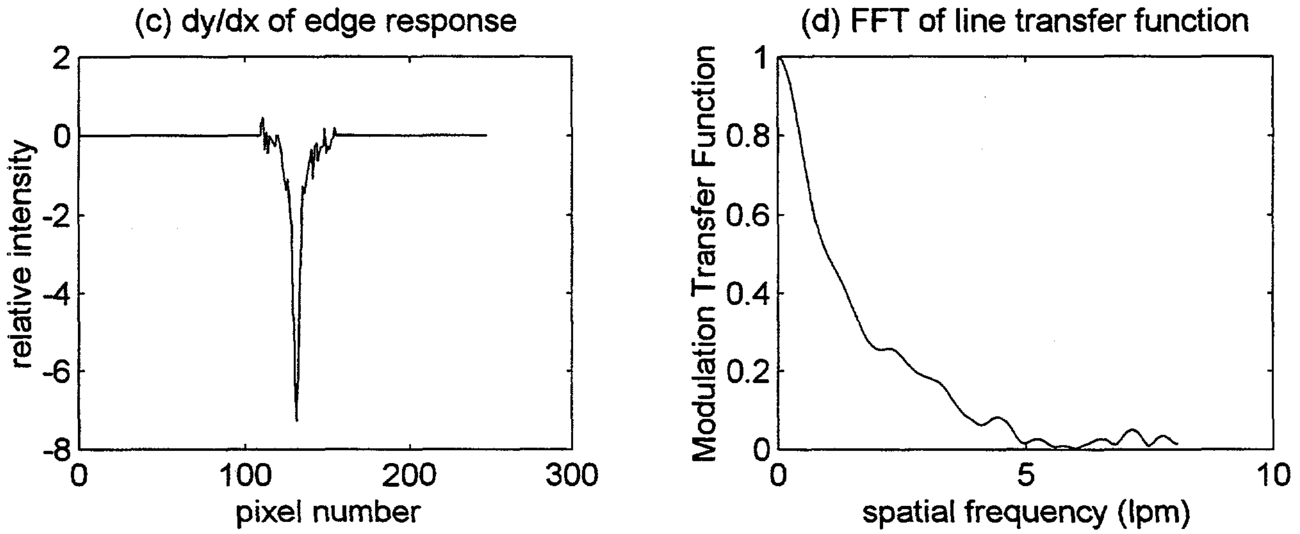

(c) dy/dx of edge response

(d) FFT of line transfer function

Figure 8. Measuring MTF using the edge response of the optical system. The optical system's response to a sharp light-to-dark transition is shown in (a). This data is modified in (b) to facilitate the FFT. The data in (b) is differentiated to obtain the line response shown in (c). The absolute value of the Fourier transform of the line response is the modulation transfer function shown in (d).

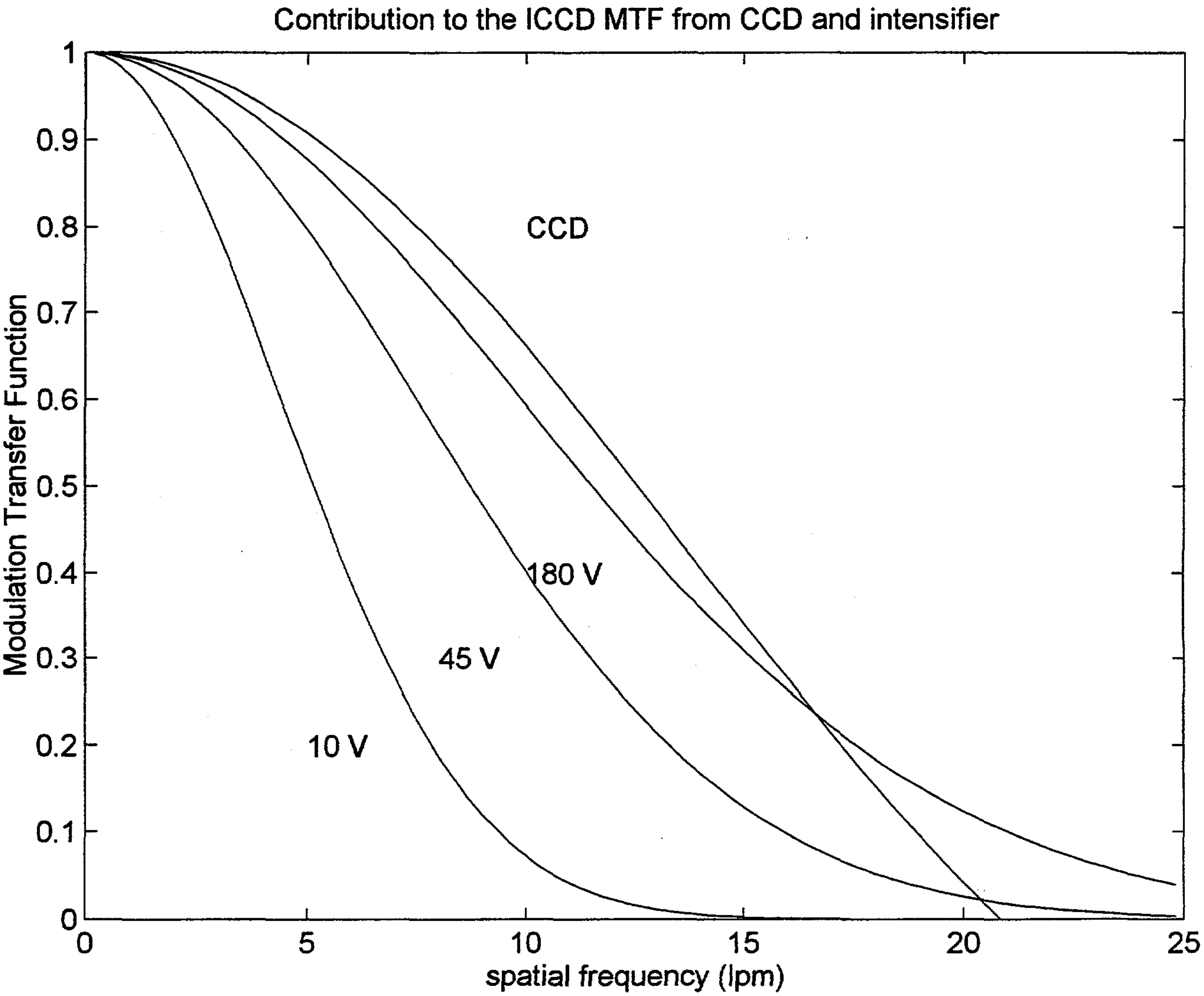

Figure 9. Contributions to the MTF of the intensified CCD (ICCD) array due to the CCD and the intensifier vs. the photocathode voltage.

photocathode voltage to just above turn-on voltage respectively. Note that the MTF of the intensifier decreases as the photocathode voltage decreases with its cutoff frequency moving from ~30 lpm at $V_{pc} = 180$ V to ~11 lpm at $V_{pc} = 10$ V. The effect of V_{pc} on the system MTF is important for us to consider since we modulate the photocathode voltage, and the average value of V_{pc} will be much less than the voltage needed for maximum MTF.

For comparison, the MTF of the CCD array (as viewed in the plane of the phosphor) is also shown in Figure 9. When the image intensifier is operating at $V_{pc} = 180$ V, its MTF is nearly equal to the MTF of the CCD. In this case, a CCD with higher resolution may improve the overall system resolution since the overall MTF is the product of the individual MTFs. However, for this project we are operating the image intensifier at much lower photocathode voltages corresponding to $V_{pc} = 45$ to 10 V. In this case the MTF of the intensifier is significantly less than that of the CCD the overall MTF is limited by the image intensifier.

The overall MTF of the ICCD system as a function of photocathode voltage and the measured MTF of the system we used for this project are plotted in Figure 10. The average operating point of our system lies somewhere between $V_{pc} = 45$ V and 10 V with a cutoff frequency ~11 lpm. The measured cutoff frequency of our system is ~5 lpm. We believe that the majority of the discrepancy between the calculated and measured MTF is due to the non-optimal coupling between the fiberoptic imaging devices that transfer the image from the output phosphor to the CCD. Since these imaging fiberoptic devices are extremely fast (NA approaching 1.0), separations of 10's of microns or more between these interfaces can cause significant degradation of the final image sharpness. It is apparent from the image data of Figure 7 (and subsequent images) that at least one of the interfaces became separated near the left-hand edge and corners of the image. The spatial resolution of our ICCD could be improved significantly by using optimized mounting hardware to positively ensure the fiber optic faceplates are in contact with one another.

Although the spatial resolution of the ICCD that we used for this work was less than ideal, we decided to concentrate our efforts on the high-frequency electronic modulation of the device, data processing, and data analysis in order achieve the primary goal of this project: to demonstrate higher range resolution from a scannerless laser radar and to see if the resulting system could play a practical role in manufacturing.

Range Resolution

Any discussion of range resolution must begin with a definition of what is meant by *range resolution*. At least two different statistical concepts are meaningful to a discussion of range resolution in ladar systems: accuracy and precision. The accuracy of a range measurement is a measure of how close a measured range is to the actual (or true) range to the target. Precision, on the other hand, is a measure of the repeatability of the ladar range measurements. Ironically, a ladar that is very

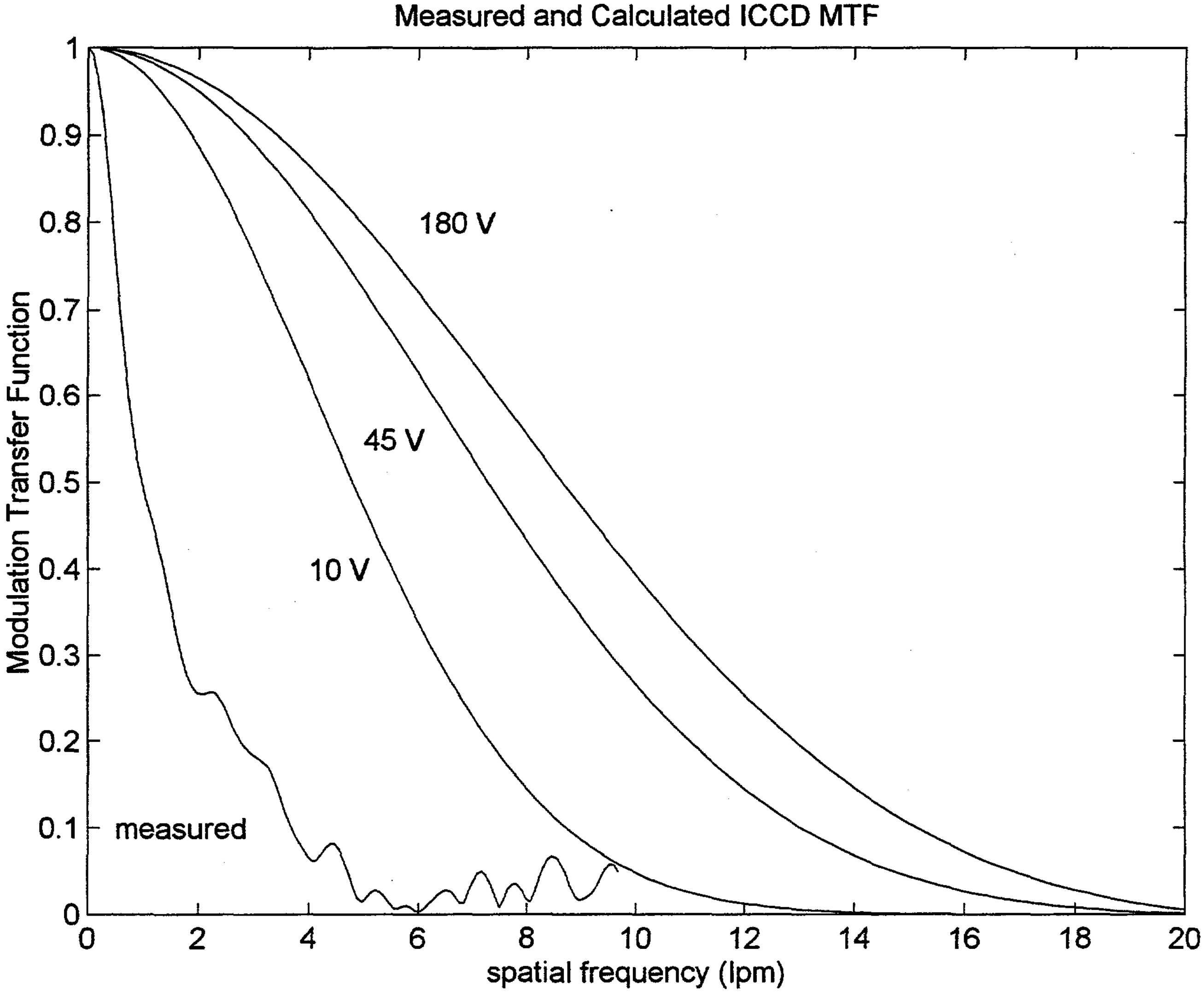

Figure 10. Comparison of the measured ICCD MTF and the calculated MTF as a function of the photocathode voltage.

precise could produce measurements that are very inaccurate. For example, a ladar with an ambiguity range of 1.0 m might have a repeatability of 1.0 mm, yet could produce range errors of 0.1 m or more due to systematic errors in calibration or lack of an absolute calibration. For ladar systems, errors in accuracy often indicate systematic errors in the system (that may be compensated for by calibrations), while the precision represents the fundamental limit of resolution for the device since it represents randomly varying noise that cannot be corrected.

There are additional complexities in our discussion of range resolution. In real scenes, the range to the target for each pixel varies over the spatial extent of the scene, and, as a result, the range resolution (however you may define it) is inextricably connected to the spatial resolution of the system. We will discuss this aspect of range resolution in more detail later in this report. To measure the range resolution of the ladar, one typically uses reference targets or scenes and compares the measured results with the known dimensions. However, the true range to any target pixel in the reference is only known to the precision and accuracy of the independent technique used to measure it. Whether one uses a tape measure, dial calipers, micrometer, or other distance measuring devices, there is always an error associated with the measurement of the true distance to the target. Ideally, this independent measurement produces an error much smaller than the errors (or noise) in the imaging ladar measurements, but this is by no means always the case.

For this project, we have concentrated on characterization of the precision of our high-frequency scannerless laser radar system, not its accuracy. We are most interested in the fundamental sources of measurement uncertainty of our system and in ways to improve it. In this report, we define the range resolution as the standard deviation in a set of range measurements to a target at a single range. There are at least two ways to measure this quantity. First, one could perform N measurements of the same scene and compute the standard deviation of the range measurements to a single pixel in the scene. This measure of range resolution demonstrates the temporal repeatability of the ladar and may be used as a gauge to the short- and long-term stability of the sensor. A second way to measure range resolution is to measure a flat target (that is, a target in which all pixels are at the same range) and compute the standard deviation of the range measurement of a patch of N adjacent pixels. Most of the work in this report uses the second method for characterizing the range resolution.

The accuracy of the high-frequency scannerless laser radar is not directly addressed in this report, although many of the measurements that we made involved targets with known range steps. From these measurements we can evaluate the ladar's ability to measure relative range in a scene. No attempt was made to calibrate our ladar in an absolute sense. Also, we have not tried to evaluate the precision of the ladar as a function of range to the target. The precision of the measurement is largely a function of the signal-to-noise ratio of the data used and should not be directly influenced by range variations encountered in a manufacturing environment. Other factors such as large variations target albedo could significantly affect SNR and, as a result, affect range precision.

Range Image Measurements of Planar Targets

The first range imaging experiments we conducted used a simple planar target oriented with its surface normal to the optical centerline of the ladar. The general experimental arrangement is shown in Figure 11. The scannerless laser radar was positioned 1.333 m from a flat panel that served as a flat background for all of the subsequent measurements. The plane of the flat target is perpendicular to the centerline of the field of view of the lens of the ladar receiver and was painted with gray-auto-body primer. The laser illuminator was positioned as close to the receiver lens as physically possible. (In scanning laser radars, the illumination beam usually is emitted from the same lens as the received light is collected.) In our data analysis, we have not corrected for the geometrical parallax that occurs because the illumination line of sight is not exactly collinear with the receiver line of sight, but we have computed its maximum effect, and found that its magnitude is much less than the range resolution of the imaging ladar.

For these and all subsequent range images, we used a 75-mm-focal-length lens on the ladar receiver. The photosensitive area of each pixel (measured at the photocathode of the image intensifier) is 48 μm by 48 μm, which represents an angular field of view of 0.640 μR (full angle) for each pixel. The photosensitive area of the receiver is 248 x 48 μm = 11.9-mm wide by 256 x 48 μm = 12.3-mm high, yielding an angular field of view of 9.1° wide (full angle) by 9.4° tall full angle). At the plane of the flat target, each pixel represents 0.853 mm by 0.853 mm. The full field of view at the flat background target is 212-mm wide by 218-mm tall.

The range image data was collected as described previously and processed using the algorithm described in Appendix B. Briefly, we collected N frames of video data of the scene in which the phase shift between the transmitter and receiver was incremented by $2\pi/N$ for each successive frame. These N frames of data were processed by an algorithm which performed a least-squares-fit to the basic CW ladar equation (Equation 3):

$$I = A + B\cos(\phi + \delta)$$

The output of the processing consisted of two images: One image contained the parameter A for each pixel which is the same as the reflectance image for the scene. The other image contained ϕ,the phase shift to the target for each pixel which is linearly related to the range to each pixel. Strictly speaking, the output image containing ϕ is a phase-shift image where the range to each pixel in the image is given by:

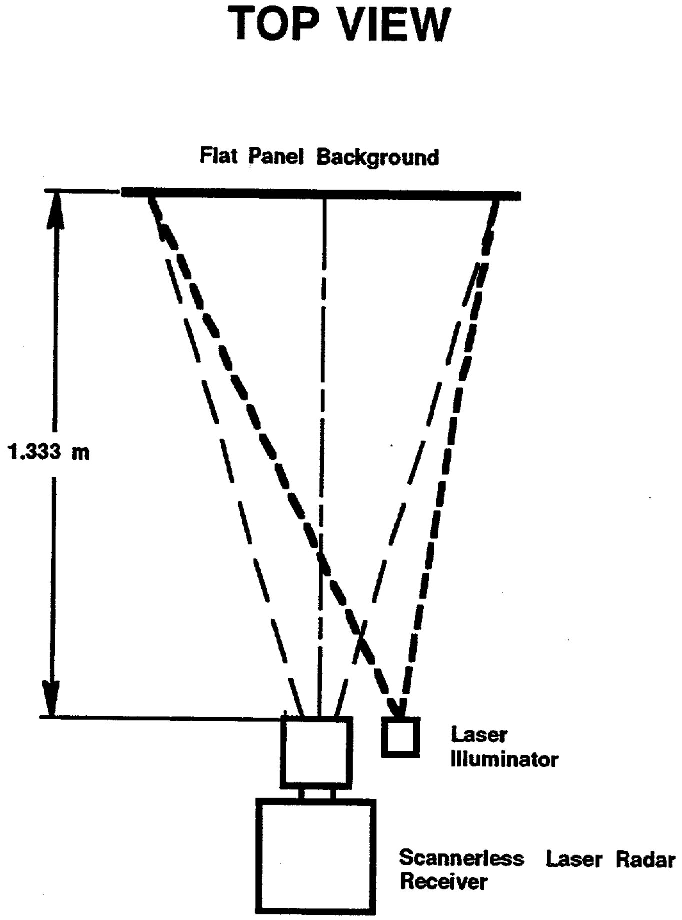

Figure 11. Optical setup for range resolution measurements on planar targets.

$$R_i = \frac{c}{4\pi f_m}(\phi_i + \phi_0) \tag{4}$$

where

c is the speed of light

f_m is the modulation frequency

ϕ_i is the measured phase shift to pixel i

ϕ_0 is a constant phase-shift offset determined for absolute calibration

In this report, we may use the terms *range image* and *phase-shift image* interchangeably. For the most part, we analyze and present results for the phase shift images even though we may refer to them as range images. Since we were not concerned with the absolute calibration of the system, we ignored the constant phase-shift offset, ϕ_0, and, as a result, our phase shift images are simply proportional to the range images.

The initial data from range images of the flat targets produced some surprising results: the range images of flat targets looked curved. Figure 12 shows a gray-scale rendering of a range image of a flat target. The gray intensity scale has been stretched to highlight the differences in range (shown as differences in intensity). Ignoring the known defects in the ICCD system on the left-hand edge and corners of the image, notice that the pattern appears most intense in the center and smoothly decreases towards the edges of the image. Figures 13-a and 13-b show a 3-D wireframe plot and a contour plot of this same data. Note that the phase-shift variation is smooth and circularly symmetric with its center near the center of the image. The peak-to-valley change in phase shift from the center of the image to the edges is approximately 25 out of 256 levels, or about 0.61 radians of phase shift (this corresponds to approximately 98 mm for our 1.0 m ambiguity level). This represents a 10% variation in measured range for a flat target.

Initially, we investigated the possibility that the perceived variation was simply due to viewing the data in an inappropriate coordinate system. The imaging laser radar measures range image data in a modified spherical coordinate system whereas we frequently view the data in a rectangular (x,y,z) coordinate system. Since the laser radar measures the range to each pixel along a line that passes through the center of the receiver lens, the edges of a planar target oriented normal to the optical centerline of the ladar field of view are actually further from the ladar than the center of the field of view. If the data from such a system is viewed without the proper coordinate transformation, the flat target will appear to be curved. (The details of the coordinate transformation from the laser radar native coordinate system to Cartesian coordinates is given in Appendix C.) However, the worst-case magnitude of this effect for our system configuration is only 0.3 %, and its direction is opposite that of the observed phase variation.

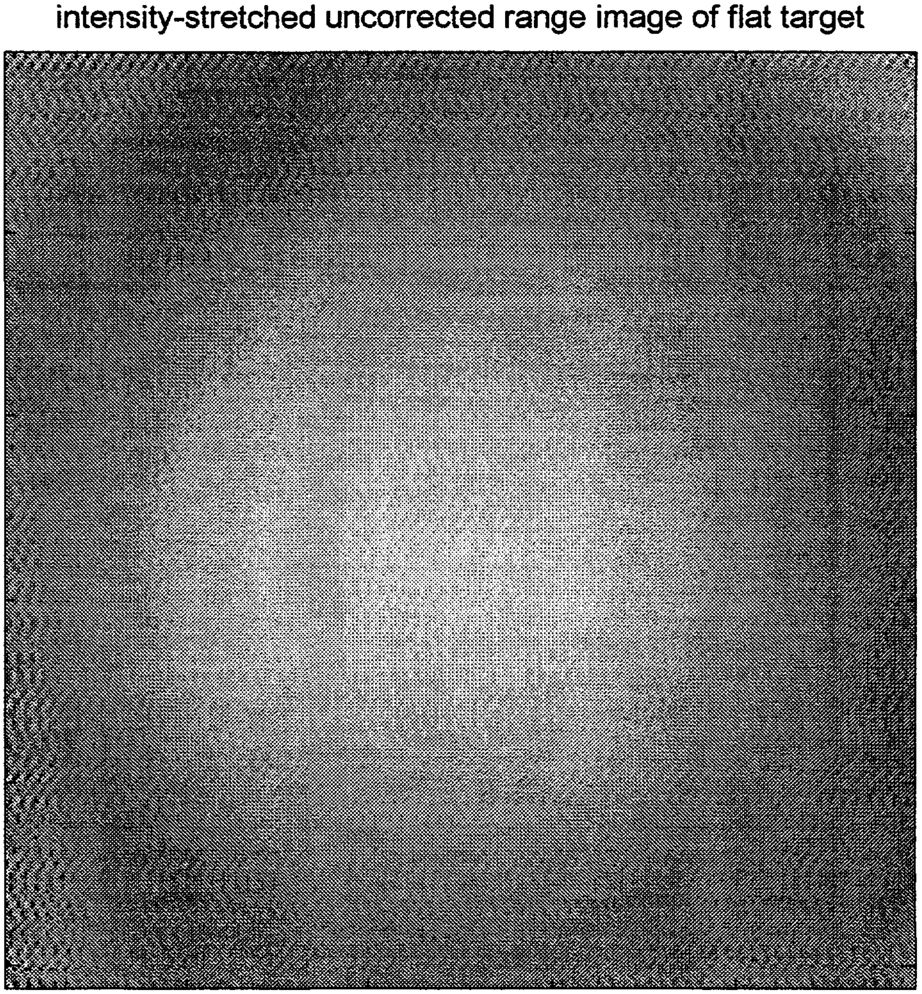

Figure 12. Uncorrected range image of a planar target. The displayed imaged has been intensity stretched to highlight the spatially varying phase shift.

(a) mesh plot of phase-shift image of flat target

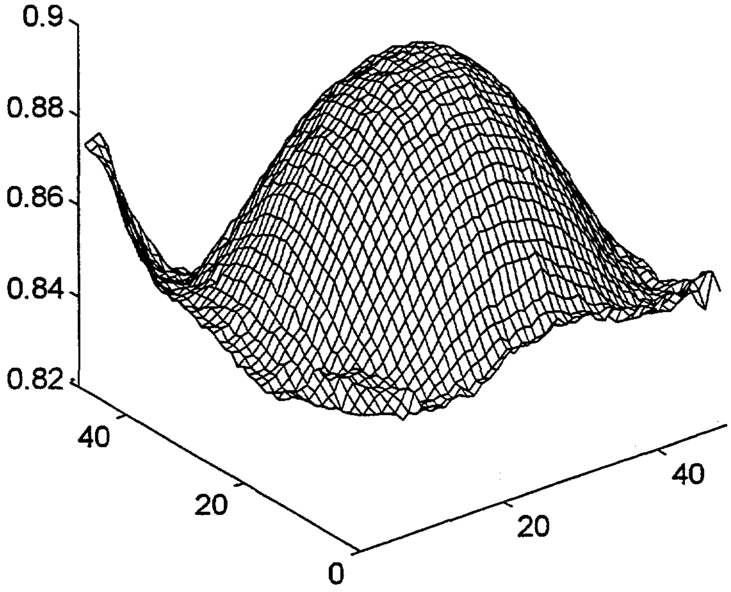

(b) contour plot of phase-shift image of flat target

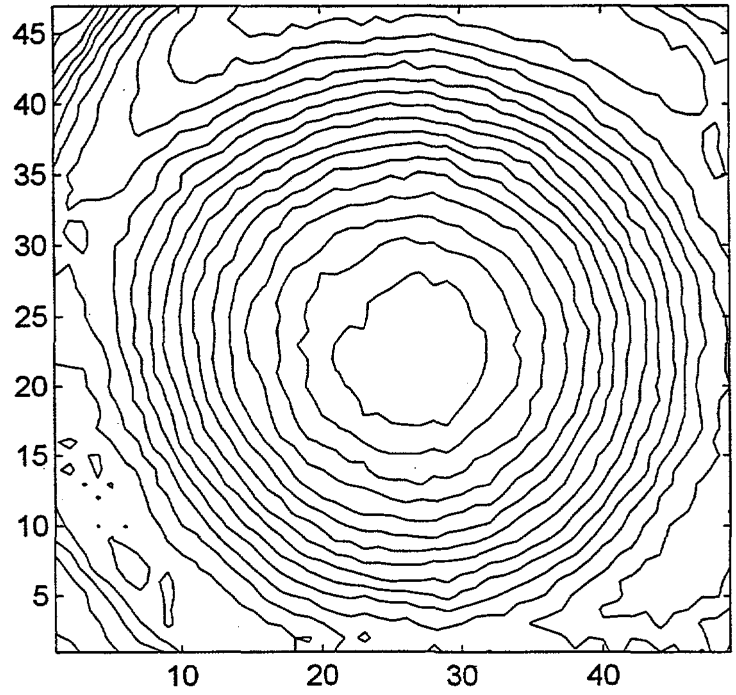

Figure 13. Mesh plot and contour plot of spatially varying phase shift seen on planar targets.

Further investigation showed that this effect is due to electrical signal propagation delay across the photocathode. The high-frequency sinusoidal voltage needed to modulate the gain of the ICCD is applied to a ~25-mm-diameter copper ring that encircles the photocathode. The photocathode itself consists of a thin coating of $(Cs)Na_2KSb$, forming an electrically conductive disk with diameter ~ 20 mm. Since the modulation voltage is applied to the outer diameter of the (copper) ring, and the photocathode has finite impedance, the sinusoidal signal experiences a phase delay as it travels from the edge of the photocathode towards the center.

In order to better understand this effect, we measured the same flat target at different modulation frequencies. The results of this measurement for modulation frequencies of 5.5, 10, 20, 40, 80, and 150 Mhz are plotted in Figure 14. These plots are profiles of the phase shift variation through the peak of the pattern. Note that the magnitude, direction, and shape of the variation are all frequency dependent. For frequencies between 5.5 and 40 Mhz, the measured phase shift for the flat target is lower in the center than the edges, and, as the modulation frequency increases, the magnitude of the peak-to-valley phase shift increases. Somewhere between 40 and 80 Mhz, the simple shape of the phase shift distribution changes, and, at 150 Mhz, its direction is opposite that at lower frequencies. At 150 Mhz, the operating frequency for most of the work described in this report, the phase shift is highest in the center of the image.

We have also observed that the magnitude, shape, and position of this phase-shift distribution is not a function of illumination level or illumination pattern. The effect does not appear to be a function of the range to the target either. Therefore, we believe that this spatial variation of phase shift is a property of the modulated image intensifier tube that can be corrected for rather simply. To correct our range images for this spatially varying phase shift, we simply subtract the phase shift pattern obtained from a standard (or reference) flat target from each phase shift image. All of the range image data presented in this report is corrected for this effect unless otherwise stated.

Range Image Measurements of Step-Range Targets

The next set of experiments were designed to measure the response of the ladar system to simple step functions of range. From this data, we can determine:

- the range resolution over areas of constant range
- how well can the ladar differentiate between two simple planar targets at different ranges.
- what is the interrelationship between spatial resolution and range resolution

The experimental setup is illustrated in Figure 5. The same flat background panel was used as before. Another flat panel was placed in front of the background panel, parallel to it, and covering approximately 50% of the field of view. This foreground panel was mounted on a slide so that the spacing between the two panels was

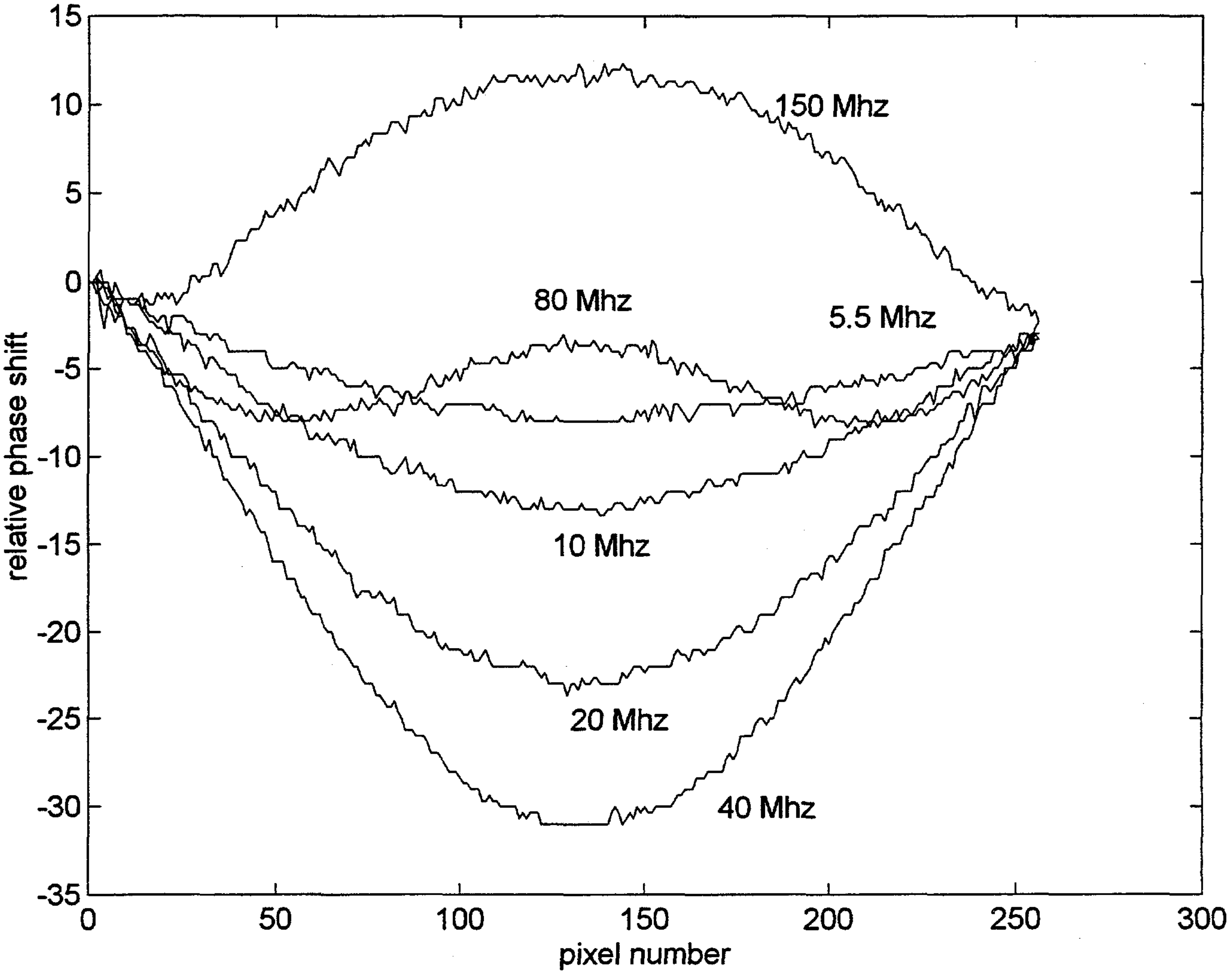

Figure 14. Spatially varying phase shift as a function of modulation frequency.

variable. We collected data sets with background-to-foreground spacing of 0.01 m, 0.02 m, 0.05 m and 0.10 m. Each raw data set was taken with N = 20, and equal phase steps of $\delta = 2\pi/20 = 314$ mR (18°). All of the N = 20 frames were used in the algorithm that produced the range and images.

A corrected phase-shift image of a data set for range step of 0.01 m is shown in Figure 15-a. For clarity, the gray scale map of this image has been stretched to highlight the differences of phase shift (range) in the scene. That is, the minimum phase shift in the entire image has been assigned the value 0 (black) and the maximum phase shift has been assigned the value 255 (white). In general, we display most range images in this report as intensity-stretched images to reveal subtle features of the image as a whole. Note the vertical line in the image marking the boundary between the background panel (on the left) and the foreground panel (on the right). The background panel appears lighter than the foreground panel since it is further away and, therefore, has greater phase shift. The subtle herringbone pattern throughout the phase-shift image is due to interference between the ~150-Mhz modulation of the ladar and the readout electronics for the CCD. The severity of this effect was a function of the modulation frequency, and we adjusted the exact modulation frequency to minimize it. We believe that, with more careful electromagnetic shielding, this effect can be virtually eliminated. Also note the portions of the image near the edges (particularly the lower left-hand edge) and corners that correspond to places where the fiber-optic coupler was not contacted to the CCD properly. These regions do not contain valid range (or video) data and have not been included in data analysis.

Our first analysis of this range-step image consisted of computing the range to each panel and then the range difference between panels. To determine the range to each panel, we selected a rectangular region for each panel and computed the average phase shift. The regions selected for analysis are indicated by boxes outlined in Figure 15-a. Each box contains 90 x 50 = 4500 pixels. In addition to the average phase shift within each box, we computed the standard deviation of the measured phase shift within each box to determine the range resolution.

A plot of the measured phase shift across the 0.01-m range step is shown in Figure 15-b. We have plotted the average of the 10 rows that cross the center of the boxes. Also, we have plotted the average phase shift (for the whole box) for reference. Figures 16, 17, and 18 show the same analysis for range steps of 0.02 m, 0.05 m, and 0.10 m respectively. The basic results from this series of measurements are summarized in Table 1. Here we show the measured range step and the standard deviation for each of the steps in so-called analog-to-digital units (ADU). For these measurements, our algorithm quantized the computed phase shift to 8-bit resolution. That is, the measured phase shift 0 to 2π is mapped to 8-bit integers 0 to 255. The measured range step as a function of the true range step is plotted in Figure 19. We have applied a least-squares fit to the data to determine the sensitivity of the system. For the data shown, the sensitivity (or relative calibration

(a) rr4a1.c08 intensity stretched image

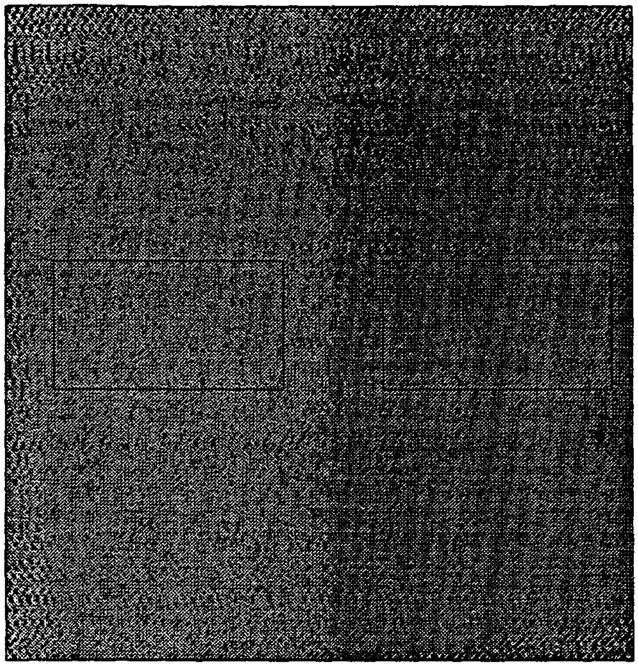

(b) rr4a1.c08 mean of center 10 rows

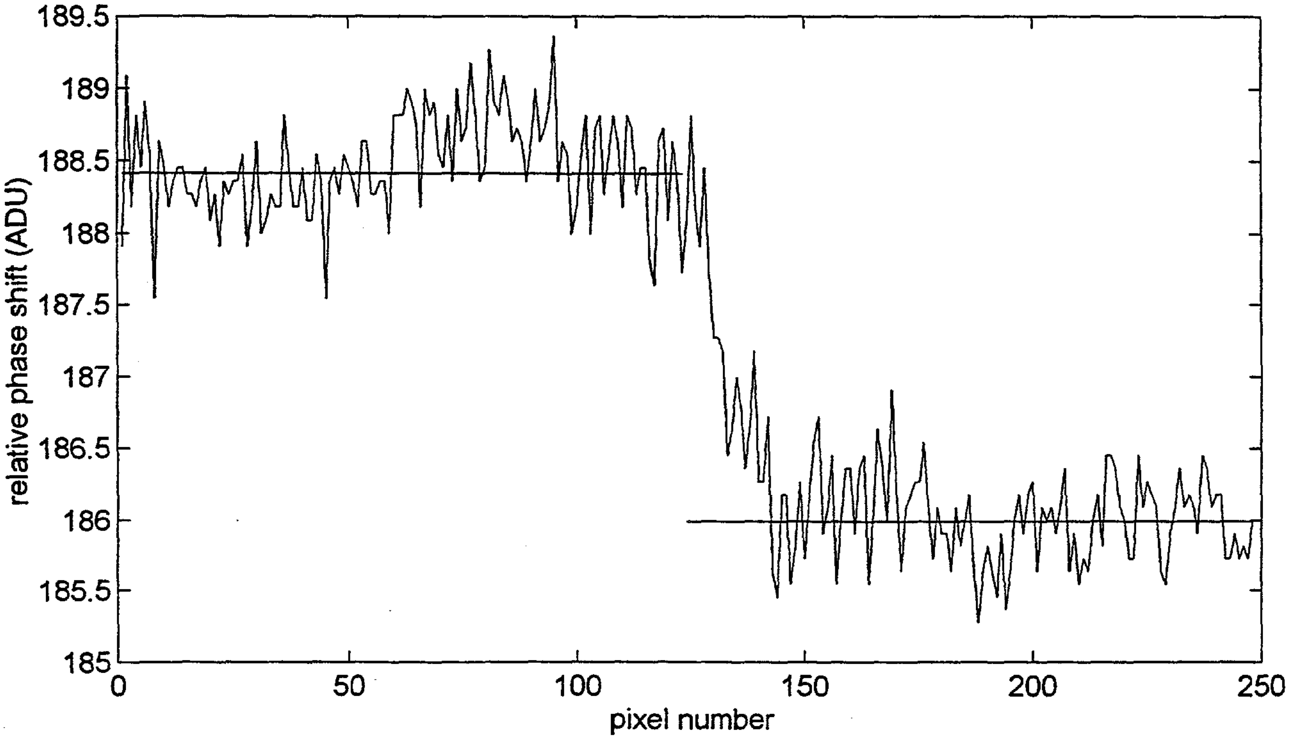

Figure 15. Data for range step target with 1.0 cm step size.

(a) rr4a2.c08 intensity stretched image

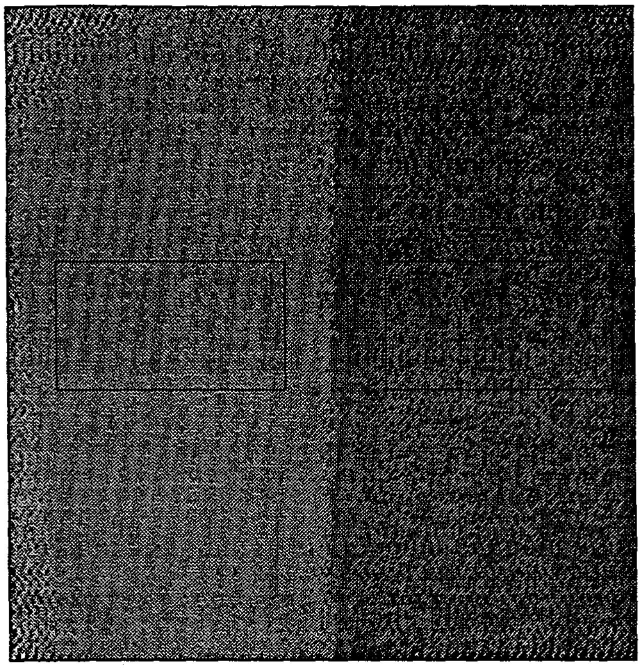

(b) rr4a2.c08 mean of center 10 rows

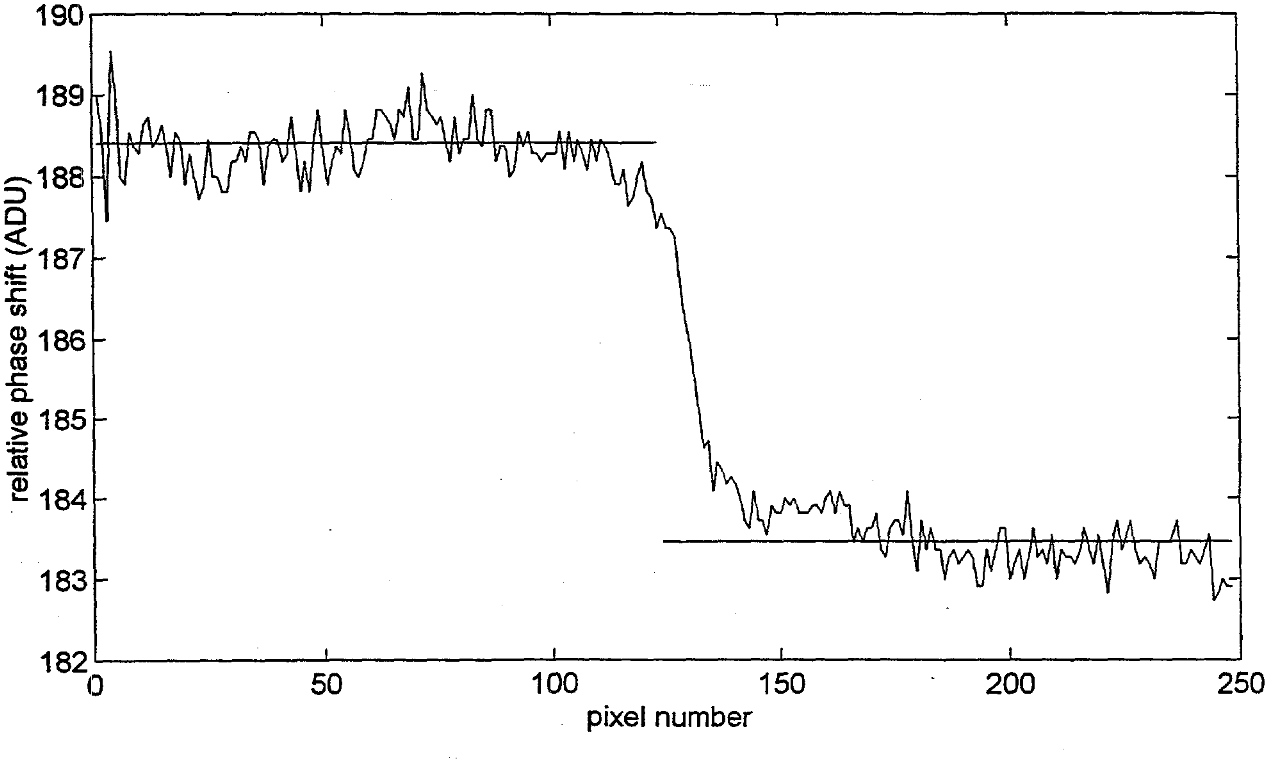

Figure 16. Data for range step target with 2.0 cm step size.

(a) rr4a3.c08 intensity stretched image

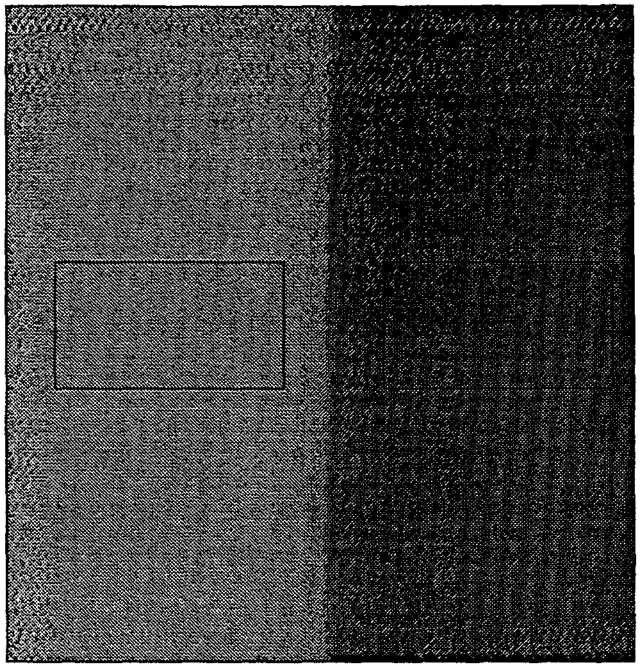

(b) rr4a3.c08 mean of center 10 rows

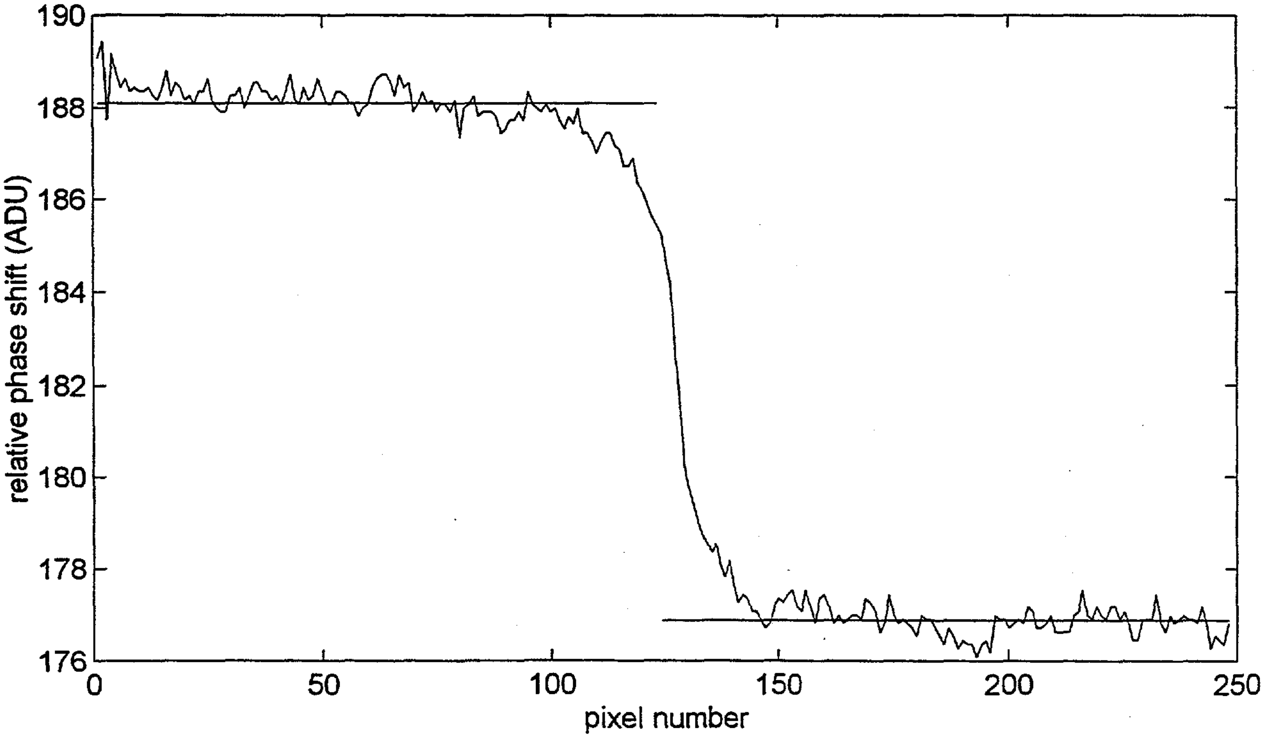

Figure 17. Data for range step target with 5.0 cm step size.

(a) rr4a4.c08 intensity stretched image

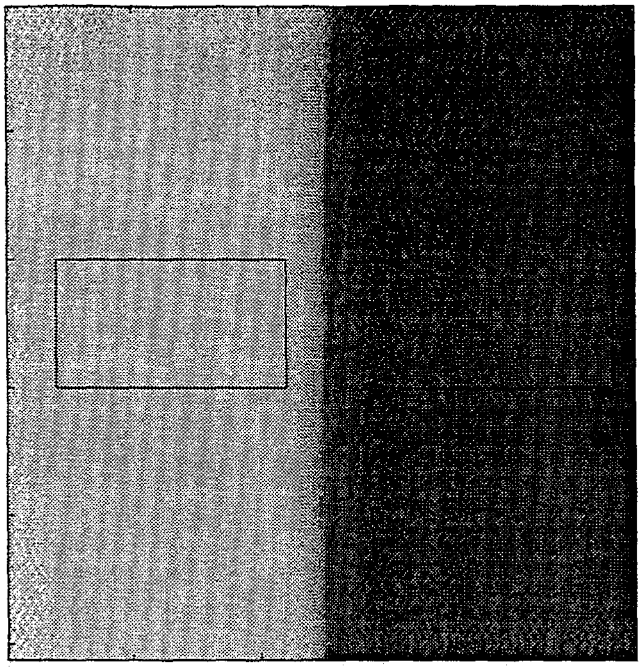

(b) rr4a4.c08 mean of center 10 rows

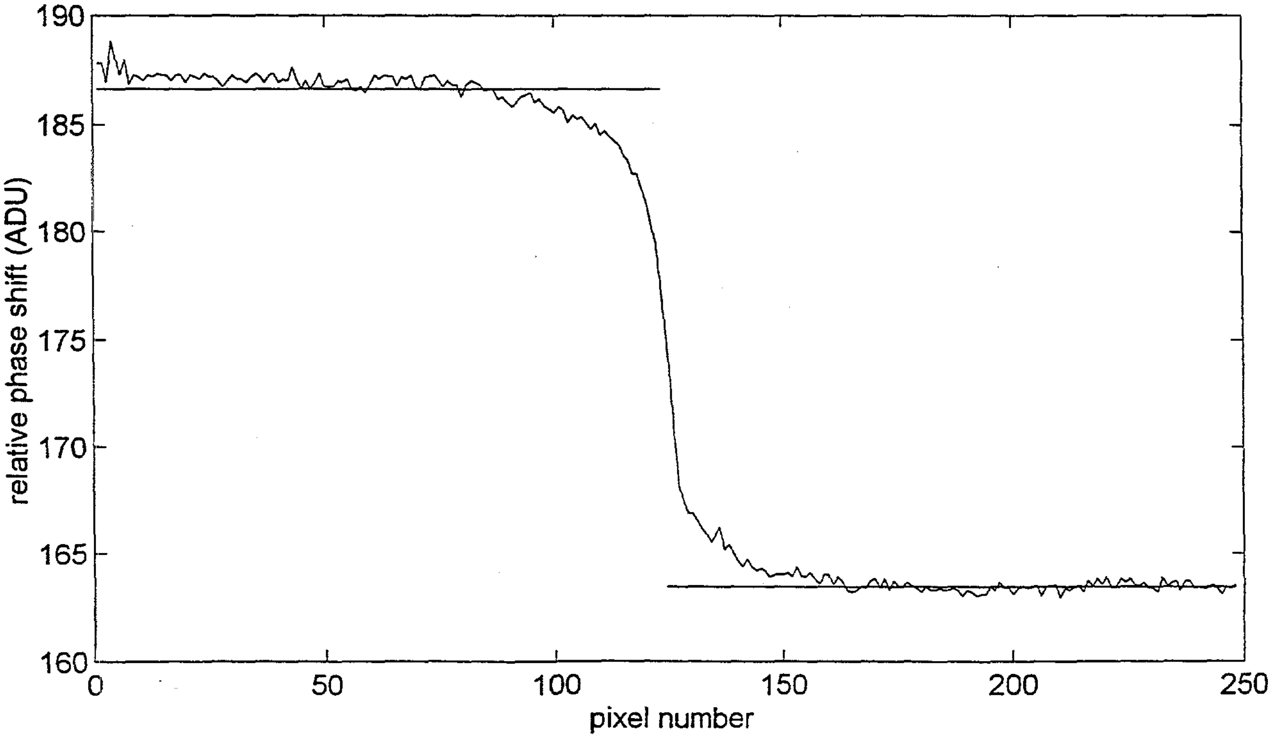

Figure 18. Data for range step target with 10.0 cm step size.

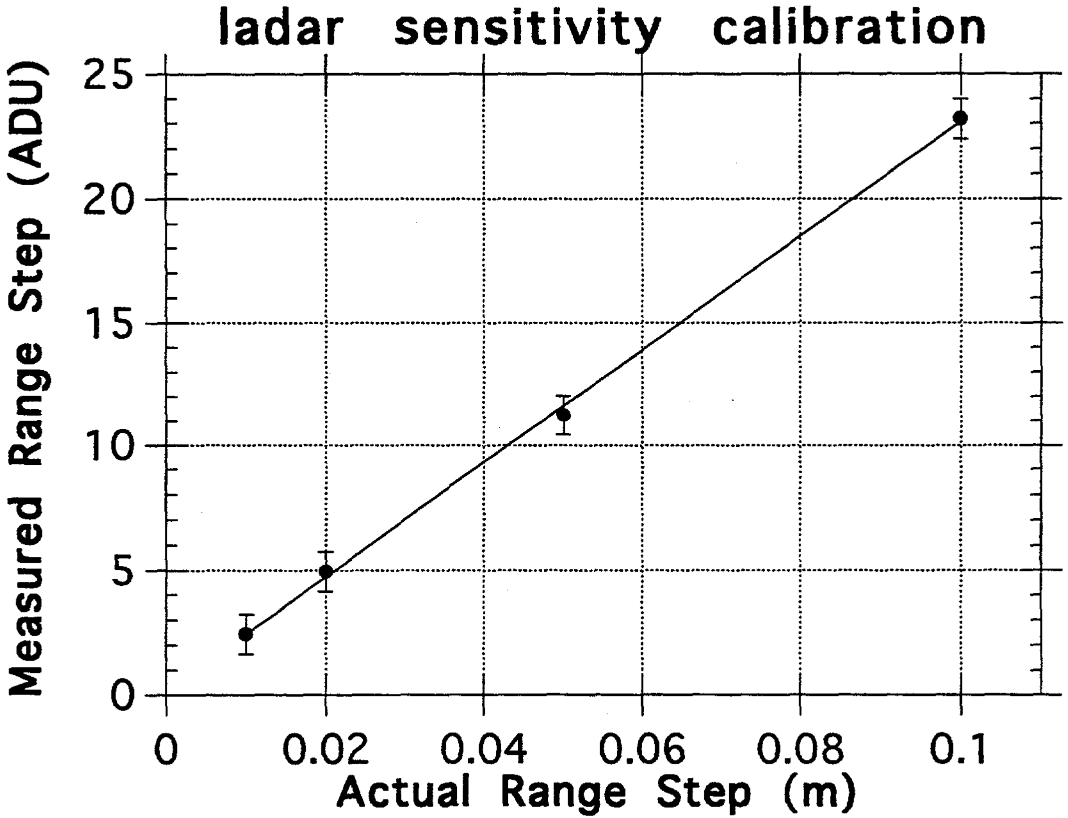

Figure 19. Calibration of the scannerless ladar sensitivity.

constant) is 4.3 mm/ADU. This corresponds to an ambiguity distance of 1.1 m or an effective modulation of 136 Mhz. (As mentioned earlier, operation at 150 Mhz produced too much interference on the range images and the actual operating frequency of the ladar was adjusted to minimize this effect.)

Table 1. Range Step and Range Resolution Data

Range Step (m)	Measured Step (ADU)	Standard Deviation (ADU)
0.01	2.4	0.80
0.02	4.9	0.80
0.05	11.2	0.79
0.10	23.2	0.87

The range step data set also contains information on the range resolution of the high-frequency ladar system. The standard deviation of phase measurements within each box was ~0.8 ADU for all of the data. This corresponds to a standard deviation of the range measurement of ~3.4 mm.

If N 8-bit-resolution images are used as raw data to compute one range image, and if the intensity errors are not correlated between the input images, we expect the resolution of the range image to improve as $\sqrt{N}$[8]. (This is equivalent to averaging N measurements to improve the signal-to-noise by $\sqrt{N}$.) As a result, the resolution of the range image may exceed the 8-bit-resolution of the data if enough raw images are used. To test this idea, we modified our phase image computation algorithm to write its result out as a 16-bit image. Normally, our algorithm first converts the 8-bit input images into floating-point images, then performs all computational steps with floating-point arithmetic, and finally writes out the result as an 8-bit range image. Thus we were arbitrarily quantizing the resultant range images to 8-bit resolution. We modified our program to write the range image as both an 8-bit and a 16-bit image so that we could compare the range resolution of the two images. As mentioned before, the 8-bit range images showed a range resolution (standard deviation of a rectangular area of 90 x 50 = 4500 pixels) of ~3.4 mm while the 16-bit range images showed range resolution of <3 mm. These comparisons were made using the same input data and same processing algorithm, and the results demonstrate that quantization error of writing the resultant range image can limit the range resolution if it is set too low. Based on the data and results from this study, the ~3-mm resolution for an ambiguity range of 1.1 m corresponds to approximately 3-parts-per-thousand precision or almost 8.5-bits resolution. Note that the 20 input images used for this study each was noisier than an ideal 8-bit image and that the intensity noise in the raw images is not totally uncorrelated.

For the performance of the hardware used in this study it is hardly worth writing out the range images at more than 8-bit resolution. However, for an optimized system with low noise input images, one should expect to generate range images with higher resolution than the input images. In fact, this is one of the two ways to improve the range resolution of the scannerless laser radar as a whole. The other factor that directly affects range resolution is the modulation frequency.

We also studied the range resolution as a function of N to see whether our system obeys the $1/\sqrt{N}$ scaling discussed earlier. We analyzed several data sets using 20, 10, and 5 frames of raw data from each set. All data sets and subsets had equally spaced phase shifts between frames, and all data was processed with the same algorithm (which reported their results in 16-bit format). Figure 20 shows the average range resolution as a function of N. Note that on this ln-ln plot, the ideal $1/\sqrt{N}$ scaling follows a slope of -1/2, while a least squares fit to our data shows a slope of -0.28. Most of the discrepancy between our system performance and an ideal system is probably due to intensity-error correlations frame-to-frame. The herringbone pattern that is evident in the raw data (due to interference between the CCD camera readout electronics and the high-frequency modulation of the image intensifier) is an example of correlated noise. Both the algorithm and the number of frames chosen to process the data will affect the range resolution. For example, common 4-frame algorithms (with 90° phase shift between frames) are particularly sensitive to correlated noise[8].

Relationship Between Range Resolution and Spatial Resolution:

The range resolution and spatial resolution of any imaging laser radar are intimately related. In most applications of imaging ladars, the scene of interest is not a plane or other simple, smooth shape, but, rather, will contain changes in range that vary across the scene. Features in the scene whose range varies on a scale smaller than the spatial resolution of the ladar will be blurred or lost completely due to the fact that the ladar is getting information from different ranges blended into one pixel. Some authors refer to this as the mixed pixel problem. That is, the pixel receives information from two or more different ranges.

The data that we have taken on simple range steps provides an ideal data set for quantitatively measuring the spatial-range resolution of our system. We perform the same analysis on the range step data as we performed on the edge response data for the ICCD reflectance images to determine the system MTF. The quantity we calculate now we will call the range image MTF. An example is shown in Figure 21. Figure 21-a shows a gray-scale image of the range data. A profile across the measured range step is shown in Figure 21-b. Unlike the reflectance data, we are not concerned with the illumination uniformity or the uniformity of the object albedo since the range images are naturally insensitive to these quantities. The plot of Figure 21-b, which we call the range-edge response, clearly shows two different ranges with a transition between them. We differentiate the range-edge response to obtain the range-line-spread function shown in Figure 21-c. The absolute value of the Fourier transform of the range-line-spread function is the range-image modulation transfer function, shown in Figure 21-d. We compare the range

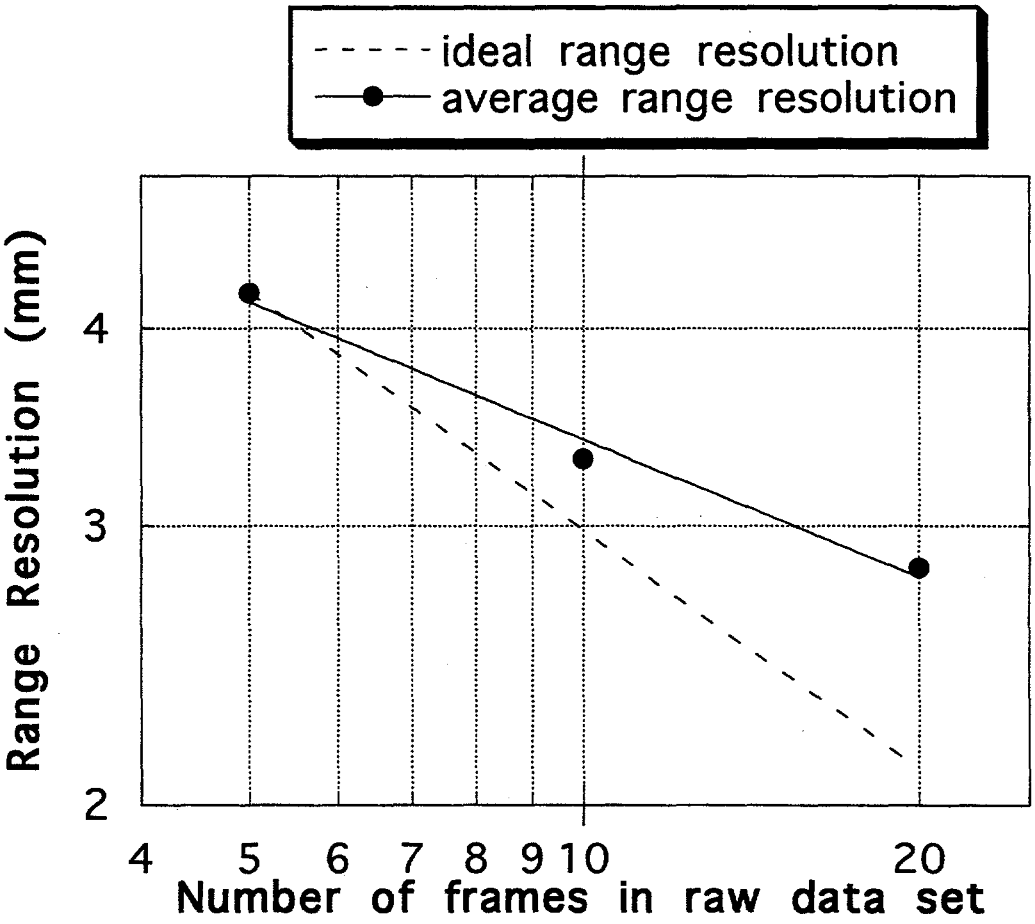

Figure 20. Range resolution as a function of number of frames of raw data.

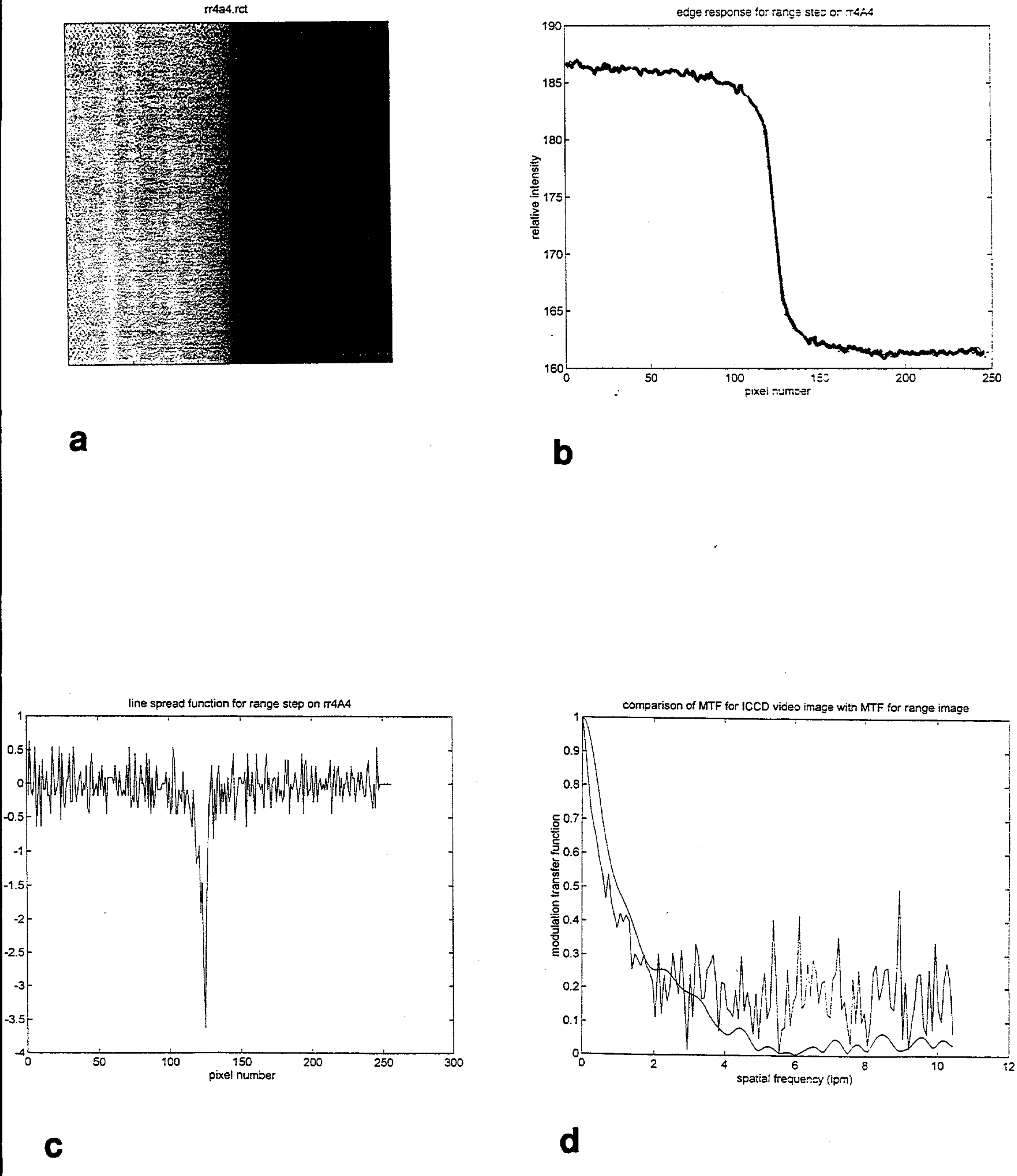

Figure 21. Calculation of the range-resolution modulation transfer function.

modulation transfer function we have just derived with the modulation transfer function we measured for the ICCD reflectance images in Figure 22. As expected, the two MTFs are nearly the same with the range MTF dropping off faster than the reflectance MTF. The range MTF can never be better than the reflectance MTF since the reflectance optical system collects the raw data for the range images. The range-image MTF is noisier than the reflectance MTF at high spatial frequency, probably due to the high-frequency noise of the range image itself.

Summary

The overall goal of this project was to assess the suitability of the scannerless imaging laser radar for inspection, measurement, and control applications in advanced manufacturing. To accomplish this, we first modified an existing 5.5-Mhz scannerless ladar to operate at modulation frequencies up to 160-Mhz, increasing its range resolution. We then adapted algorithms from the field of phase-shifting interferometry to process our data and achieve further improvements in range resolution through better SNR. During the course of this project, we observed a frequency and spatially dependent phase shift due to the signal propagation delay across the image intensifier, and we developed a method to correct range images for this significant systematic error. Finally, using the high-frequency ladar and the new algorithms, we measured the spatial and range resolution of the system.

The results of our study show that we have improved the range resolution of the scannerless laser radar by nearly a factor of 100. The range resolution of our high-frequency system is currently ~3 mm using 20 frames of input data. The new data processing algorithms that we developed will allow existing and future ladars to perform with higher range resolution. In addition, we gained valuable experience in approaching the electronic subtleties that occur when the ladar system is operated at high frequencies. Finally, we developed a variety of new analysis tools for evaluating range image data.

Although the hardware configuration used in project did not achieve our initial goal of 1-mm range resolution, our demonstration of 3-mm resolution does make the scannerless laser radar a candidate for an inspection and measurement sensor for manufacturing. We believe that an optimized system operating at a modulation frequency of 300 Mhz or greater could have a range resolution approaching 1.0 mm. In addition, the spatial resolution could be improved by optimum optical coupling of the image intensifier to CCD.

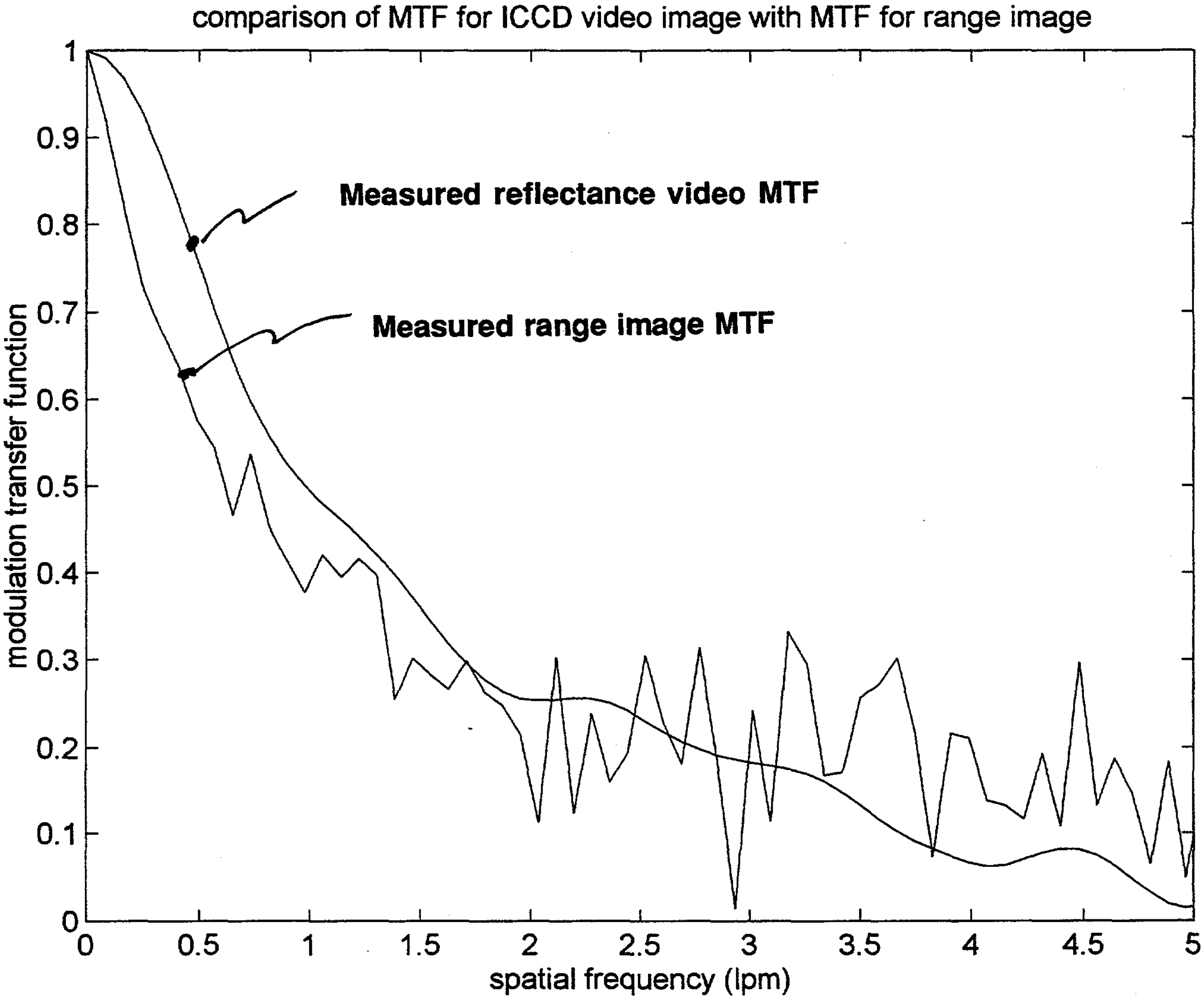

Figure 22. Comparison of measured ICCD MTF and measured range-resolution MTF.

Based on the results of this project, we believe that an optimized scannerless laser radar could be a useful industrial inspection, measurement, and process control tool for applications requiring range resolution of approximately 1 mm. In order to achieve this level of performance, the scannerless laser radar would have to be redesigned for even higher modulation frequencies and implemented using optimized optical coupling of the image intensifier to the CCD. In addition, a new system would employ a low-noise CCD to minimize the errors associated with digitizing the raw phase information from the scene. Real-time data reduction could be realized by implementing already-developed data reduction algorithms from the field of phase-stepping interferometry on DSP hardware on a standard personal computer (such as a Pentium-based PC).

References:

1.) M. W. Scott, "Range imaging laser radar," United States Patent no. 4,935,616 issued June 19, 1990.

2.) J. P. Anthes, P. Garcia, J. T. Pierce, P. V. Dressendorfer, "Nonscanned ladar imaging and applications," in *Applied Laser Radar Technology*, G. W. Kammerman and W. E. Keicher, Editors, Proc. SPIE **1936**, 11 (1993).

3.) P. Garcia, J. P. Anthes, J. T. Pierce, P. V. Dressendorfer, I. K. Evans, B. D. Bradley, J. T. Sackos, and M. M. Lecavalier, "Characterization of a scannerless ladar system," in *Applied Laser Radar Technology*, G. W. Kammerman and W. E. Keicher, Editors, Proc. SPIE **1936**, 23 (1993).

4.) C. S. Williams and O. A. Becklund, Introduction to the Optical Transfer Function, John Wiley and Sons, 1989.

5.) J. W. Goodman, Introduction to Fourier Optics, McGraw Hill, 1968.

6.) J. D. Gaskill, Linear Systems, Fourier Transforms, and Optics, John Wiley and Sons 1978.

7.) P. H. Paul, "The application of intensified array detectors to quantitative planar induced-fluorescence imaging," paper AIAA 91-2351 presented at the AIAA 27th Joint propulsion conference, Sacramento, CA (1991).

8.) C. P. Brophy, "Effect of intensity error correlation on the computed phase of phase-shifting interferometry," J. Opt. Soc. Am. A, 7, 537, 1990.

Appendix A: Overview of Scannerless Laser Radar

Introduction

Just a few years after the invention of the laser, workers at Hughes Aircraft demonstrated the first application of pulsed lasers for distance measurement[A1]. By photographically recording oscilloscope traces of the output pulse from a ruby laser and its subsequent echo from the remote target, they were able to measure the distance to the target. Now, over 30 years later, laser rangefinder technology has matured, and a variety of instruments are commercially available. For many applications, however, the state-of-the-art in laser rangefinders are still relatively primitive -- data acquisition rates are too slow for three-dimensional imaging required for industrial applications, and the equipment is often too delicate and bulky for many applications.

Sandia's scannerless range imager is a unique implementation of continuous wave (cw) laser radar. The principle of cw radar, illustrated in Figure A1, relies on measurement of the phase difference between an intensity-modulated probe beam and its return from the target. The range to the target, R, is calculated from

$$R = \frac{c\phi}{4\pi f_m} \qquad \text{(A1)}$$

where c is the speed of light, ϕ is the round-trip phase shift, and f_m is the modulation frequency. In a cw ladar (or radar), the range resolution is limited by the resolution to which the relative phase shift of the return signal can be measured.

Sandia has developed and patented a unique implementation of an imaging laser radar without any scanning components[A2,A3]. Shown schematically in Figure A2, the scannerless laser radar illuminates the entire field of view at once with sinusoidally intensity modulated laser light. Light scattered from the scene is collected by a lens and imaged onto a microchannel plate image intensifier tube. The gain of the image intensifier is modulated synchronously with and at the same frequency as the laser illuminator, and the optical output of the modulated image intensifier tube is then integrated and recorded by a two-dimensional charge coupled device (CCD) detector. Each pixel in the CCD then contains information about the phase shift (and thus the range) to its image point in the scene. In essence, the scannerless range imager is a phase sensitive detector that operates on an entire image simultaneously (256 x 256 or about 65,000 pixels in our case) instead of raster scanning and sequentially measuring the phase shift to each pixel in the image.

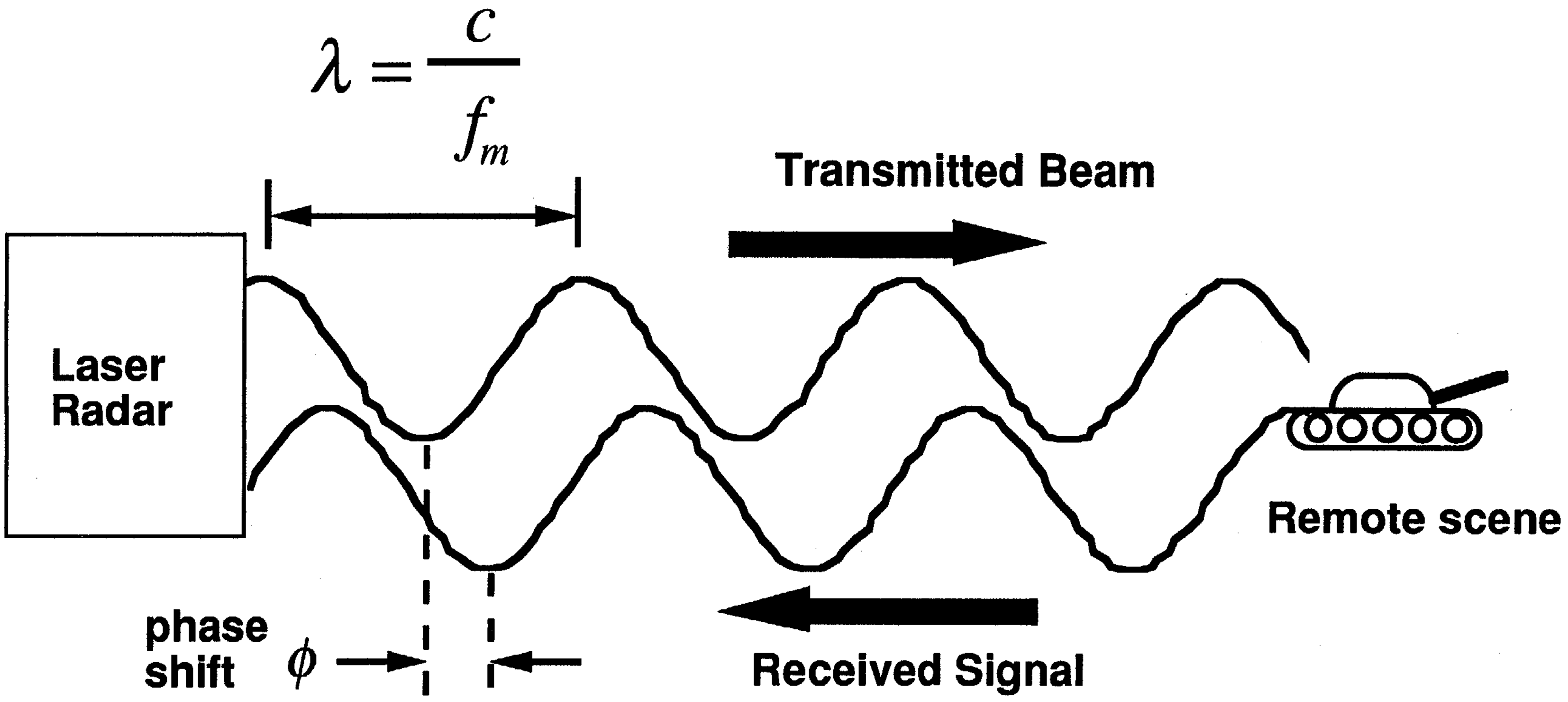

$$R = \frac{c\,\phi}{4\pi\, f_m}$$

Figure A1. Conceptual view of continuous wave (cw) laser radar. CW laser radar works by measuring the relative phase shift between a transmitted modulated signal and the signal received after reflection from the object of interest. The range to the target, R, is calculated from $R = \frac{c\phi}{4\pi f_m}$ where c is the speed of light, ϕ is the round-trip phase shift, and f_m is the modulation frequency.

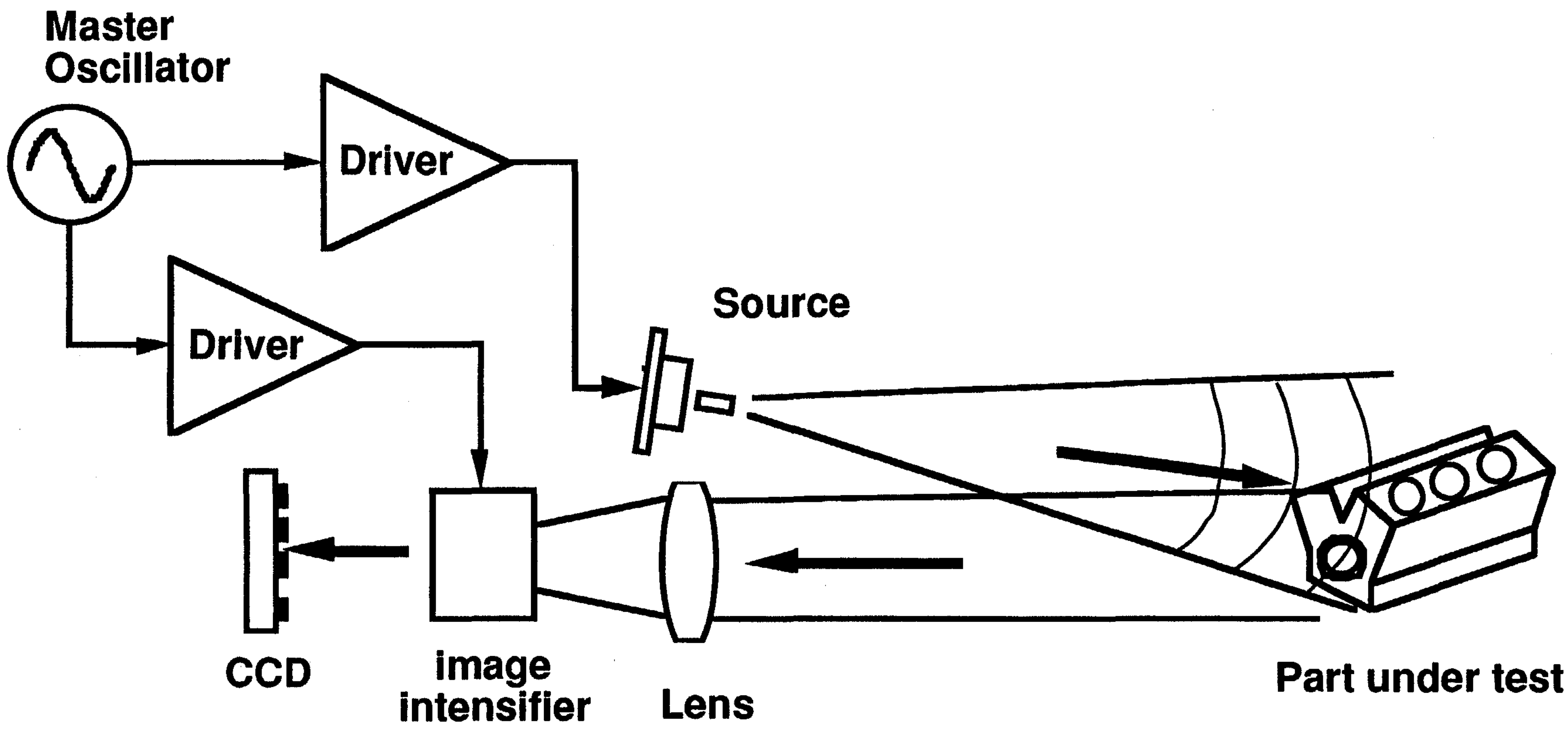

Figure A2. Schematic diagram of a scannerless laser radar system. A laser diode illuminates the entire field of view at once with sinusoidally intensity modulated laser light. Light scattered from the scene is collected by a lens and imaged onto a microchannel plate image intensifier tube. The gain of the image intensifier is modulated synchronously with and at the same frequency as the laser illuminator, and the optical output of the modulated image intensifier tube is then integrated and recorded by a two-dimensional charge coupled device (CCD) detector. Each pixel in the CCD contains information about the phase shift (and thus the range) to its image point in the scene.

The scannerless laser radar has several significant advantages over scanning systems. First, its lack of moving parts makes the scannerless system more rugged and more compact than its scanned counterparts. Also, since the entire field of view is illuminated and imaged at one time, pixel registration is fixed and well-known. Finally, the scannerless laser radar produces two images of the scene that are pixel registered with respect to one another: a range image of the scene and a laser-illuminated reflectance image of the scene.

Scannerless Laser Radar Theory of Operation

Continuous wave (cw) rangefinders work by measuring the phase difference between an intensity-modulated transmitted laser beam and its return from the target. As shown in Figure A1, the spatial wavelength, λ, of the sinusoidally modulated beam is given by

$$\lambda = \frac{c}{f_m} \qquad \text{(A2)}$$

where c is the speed of light and f_m is the modulation frequency. The light travels from the transmitter to the target, and some of the light is backscattered by the target and collected by the receiver optics. In its round trip to the target and back, the light acquires a phase shift relative to the transmitted beam of

$$\phi = \frac{4\pi f_m R}{c} \qquad \text{(A3)}$$

where R is the distance (range) to the target. In order to measure the range to the target, the cw rangefinder measures the relative phase shift, ϕ, and computes the range using equation A1:

$$R = \frac{c\phi}{4\pi f_m}.$$

Since relative phase is a periodic function (with period 2π), ranges that produce round-trip phase shifts of $\phi \geq 2\pi$ are not distinguishable from ranges with phase shifts $\phi - 2\pi$. Thus, with a cw rangefinder, one must ensure that the modulation frequency is selected to produce unambiguous range measurements for the expected maximum range interval. In cw radar, it is common to define an ambiguity interval, R_{amb}. This is the range interval over which the round-trip phase delay will be $\phi \leq 2\pi$, and distance measurements will be unambiguous. R_{amb} is given by

$$R_{amb} = \frac{c}{2f_m} = \frac{\lambda}{2} \qquad \text{(A4)}$$

The heart of any cw laser rangefinder is its phase shift detector: the more precise the phase detector, the more precise the range measurements will be. Most cw rangefinders have borrowed electronic phase detection circuits from the technologically mature field of microwave radar. In these rangefinders, the optical return signal is converted into an electrical signal (usually with a photodiode), and the phase of this electrical signal is compared to a reference signal by an electronic circuit. The primary advantage of this approach is that electronic phase measurement techniques and equipment are well developed from the cw radar and communications fields. Its primary disadvantage is the fact that conventional electronic phase meters can measure the range to only one pixel in the object scene at a time, and, as a result, the laser beam must be scanned over the scene to produce a three-dimensional image of the scene.

Sandia's solution to this problem was to develop a phase detector capable of processing all pixels in a scene simultaneously, thereby eliminating the need for scanning optics. Our phase detection technique, based on optical predetection mixing[A2], has been integrated into a patented approach for scannerless range imaging[A3]. It uses the photodetector itself as a mixer (or demultiplexer) by modulating the gain of the photodetector synchronously with the transmitted beam. This two-dimensional phase detector can be implemented with an image intensifier tube as the demodulator and a CCD array as the integrator, both commercially available components.

The scannerless range imaging concept is shown schematically in Figure A2. The transmitted beam consists of an intensity-modulated laser beam with output power of the form

$$P_t = P_0\left[1 + m_l \sin(\omega t)\right] \qquad \text{(A5)}$$

where P_t is the transmitted laser power, P_0 is the average laser power, and $\omega = 2\pi f_m$. The factor m_l is the illumination depth of modulation index. The value of m_l lies between 0 and 1. The sinusoidally modulated light travels to the scene, and some of the light is backscattered from the objects in the scene. The received optical power , P_r, is given by:

$$P_r = P_a\left[1 + m_l \sin(\omega t + \phi)\right] \qquad \text{(A6)}$$

where P_a is the average received power and ϕ is the relative phase shift between the transmitted beam and the received optical power. The factor P_a accounts for the reflectivity of the object, the collection efficiency of the optical system, the $1/R^2$ return signal dependence, and other system parameters. In order to calculate the range to a given object pixel, the phase shift ϕ must be measured. In our system, the received optical power is imaged onto an image intensifier tube in which the gain is modulated at the same frequency as (and synchronously with) the transmitted laser beam. The gain of the image tube is described by:

$$G = G_0(1 + m_g \sin(\omega t)) \qquad \text{(A7)}$$

where G_0 is the average gain, and m_g is the depth of modulation of the gain. Here $0 \le m_g \le 1$. The output of this modulated image intensifier tube is integrated on a CCD array detector with responsivity R for an integral number of periods of the modulation frequency. The signal at a pixel in the CCD is then given by:

$$I = \int_0^{nT} R G_0 (1 + m_g \sin(\omega t)) P_a (1 + m_l \sin(\omega t + \phi))dt \qquad \text{(A8)}$$

$$I = nT R G_o P_a (1 + \tfrac{1}{2} m_g m_l \cos(\phi)) \qquad \text{(A9)}$$

Equation A9 can be rewritten as

$$I = A + B\cos(\phi) \qquad \text{(A10)}$$

where A represents the average illumination intensity in the absence of modulation
B is a factor that describes the depth of modulation due to optical mixing in the image intensifier tube, and
ϕ is the phase shift to the pixel in the scene

Thus, each pixel of the CCD array contains information needed to retrieve the range-dependent phase shift, ϕ, but does not contain the phase shift directly. Since there are three unknowns in equation A10, we need at least three measurements to determine the unknowns. There are a variety of ways to retrieve the phase shift from the scannerless laser radar data. For the work in this project, we performed $N \ge 3$ measurements of the scene and used a least squares method to calculate the parameters of most interest to us: A and ϕ. The details of that analysis are given in Appendix B.

Appendix A References:

A1. M. L. Stitch, "Laser Rangefinding," in *Laser Handbook, Volume 2*, edited by F. T. Arecchi and E. O. Dubois, North Holland Publishing 1972.

A2. M. Scott and P. Garcia, "Use of predetection mixing of intensity modulated optical beams," Appl Opt **27**, 5119 (1988).

A3. M. W. Scott, "Range imaging laser radar," United States Patent no. 4,935,616 issued June 19, 1990.

Appendix B: Algorithms for Computing Range Images from Phase Shifted Images

The following appendix provides a brief description of the algorithms used to transform the raw data from the scannerless range imager into range images. The algorithms we used for this work are based on algorithms developed in the field of phase shifting interferometry[B1]. Interferometry, as used for testing of optical components such as mirror and lens surfaces, seeks to provide a map of the relative phase shift of an optical beam over the surface of the optic. One particularly sensitive technique for producing this phase shift map is phase-shifting interferometry (PSI). PSI relies on recording a number of interferograms, each with a different phase shift between the reference beam and the probe beam. This series of interferograms is then processed by an algorithm to produce an accurate phase-shift map of the optic.

The similarities between the data and data processing required for PSI and scannerless laser radar are striking. Both seek to produce a phase-shift map of the field of view of the sensor -- in the case of scannerless laser radar, this phase-shift map is directly proportional to the range to each pixel in the scene. Also, the fundamental equation describing the phenomena in both cases are identical. In each case the intensity of the recorded light is given by an equation of the form

$$I = A + B\cos(\phi + \delta) \qquad \text{(B1)}$$

where A is a constant offset proportional to the illumination intensity, $1/R^2$, the object albedo, and the optical receiver gain

B is a constant that defines a depth of modulation or modulation contrast

ϕ is the phase shift to pixel in the scene, and

δ is an electronic phase shift between the transmitted and received signal.

Because of the similarity between the data and phenomenology in PSI and scannerless laser radar, we can take advantage of the well-developed PSI algorithms to reduce and analyze our scannerless laser radar data.

The following describes a general least squares approach to computing the phase shift to each pixel using phase-stepping techniques. This section closely follows the derivation contained in reference B1.

If a series of N images are recorded with phase shifts δ between the transmitter and receiver, the intensity of a pixel in the ith image can be written as:

$$I_i = A + B\cos(\phi + \delta_i) \qquad \text{(B2)}$$

or, equivalently,

$$I_i = a_0 + a_1\cos(\delta_i) + a_2\sin(\delta_i) \qquad \text{(B3)}$$

where

$a_0 = A$

$a_1 = B\cos(\phi)$

$a_2 = -B\sin(\phi)$

The squared difference between the measured intensities and the intensities computed with equation B3 is:

$$error^2 = \sum_{i=1}^{N}\left[I_i - a_0 - a_1\cos(\delta_i) - a_2\sin(\delta_i)\right]^2 \tag{B4}$$

The error is minimized by differentiating equation B4 with respect to each of the unknowns (a_0, a_1, and a_2) and setting these equal to zero. The solution of this set of equations is written in matrix form as:

$$\begin{bmatrix} a_0 \\ a_1 \\ a_2 \end{bmatrix} = \mathbf{A}^{-1}(\delta_i)\mathbf{B}(\delta_i) \tag{B5}$$

where

$$\mathbf{A}(\delta_i) = \begin{bmatrix} N & \sum\cos(\delta_i) & \sum\sin(\delta_i) \\ \sum\cos(\delta_i) & \sum\cos^2(\delta_i) & \sum\cos(\delta_i)\sin(\delta_i) \\ \sum\sin(\delta_i) & \sum\cos(\delta_i)\sin(\delta_i) & \sum\sin^2(\delta_i) \end{bmatrix} \tag{B6}$$

and

$$\mathbf{B}(\delta_i) = \begin{bmatrix} \sum I_i \\ \sum I_i\cos(\delta_i) \\ \sum I_i\sin(\delta_i) \end{bmatrix} \tag{B7}$$

Once the values of a_0, a_1, and a_2 are known, the phase shift to the scene pixel is given by:

$$\phi = \arctan\left(\frac{-a_2}{a_1}\right) \tag{B8}$$

Note that for a given data set, the matrix **A** is only dependent on the electronic phase shifts δ_i and therefore need only be calculated and inverted once for each image. The matrix **B** must be calculated for each pixel in the image.

One case of special interest occurs when the phase shifts δ_i are evenly spaced from 0 to 2π. That is, if there are N phase shifted images with phase shifts

$$\delta_i = i\frac{2\pi}{N} \qquad i = 1,2\ldots N \tag{B9}$$

In this case, all of the off-diagonal elements of matrix **A** are zero and the phase shift is given by:

$$\phi = \arctan\left(\frac{-\sum I_i \sin(\delta_i)}{\sum I_i \cos(\delta_i)}\right) \tag{B10}$$

Note that the arctan function returns a value of ϕ between -π/2 and π/2. We do have enough information, however, to determine the value of ϕ over a full 0 to 2π region since we know the value of sin(ϕ) and cos(ϕ). The following table summarizes the correction to the value of ϕ required to achieve a full 0 to 2π phase shift range:

Modulo 2π phase correction		
sin(ϕ)	cos(ϕ)	corrected phase
0	+	0
+	+	ϕ
+	0	π/2
+	-	ϕ+ π/2
0	-	π
-	-	ϕ+ π
-	0	3π/2
-	+	ϕ+ 2π

In the above analysis, we calculated the phase shift to each pixel in the scene. The range image is computed simply by applying the laser radar equation

$$R = \frac{c\phi}{4\pi f_m} \tag{B11}$$

to each of the pixels in the phase shift image.

A reflectance image may be calculated by simply averaging the N raw data frames. Each pixel reflectance value is given by:

$$reflectance = \frac{1}{N}\sum I_i \tag{B12}$$

It is useful to define a modulation index, γ, that measures depth of modulation of scannerless laser radar at each pixel location. This is analogous to fringe contrast in interferometry. Using the same notation as in equation B1, we define the modulation index as:

$$\gamma = \frac{B}{A} \tag{B13}$$

For the previous example in which the phase shifts between input images are equal and evenly distributed from 0 to 2π, the modulation index is given by:

$$\gamma = \frac{2\left\{\left[\sum I_i \cos(\delta_i)\right]^2 + \left[\sum I_i \sin(\delta_i)\right]^2\right\}^{1/2}}{\sum I_i} \tag{B14}$$

The modulation index γ may be used as a metric to determine the reliability of the phase shift calculation of ϕ. In addition, it may be used as a diagnostic tool to assess the performance of the transmitter modulation and the receiver modulation.

This appendix has discussed only the rudimentary concepts of applying phase-shifting interferometry to collecting and processing scannerless laser radar data. References B1-B3 discuss a variety of algorithms in detail, discussing the relative merits of each technique.

Appendix B References:

B1. J. E. Greivenkamp and J. H Bruning, "Phase Shifting Interferometers," Chapter 14 in Optical Shop Testing, Edited by D. Malacara, John Wiley and Sons, 1992.

B2. C. P. Brophy, "Effect of intensity error correlation on the computed phase of phase-shifting interferometry," J. Opt. Soc. Am. A, 7, 537, 1990.

B3. K. Freischlad and C. L. Koliopoulos, "Fourier description of digital phase-measuring interferometry," J. Opt. Soc. Am. A, 7, 542, 1990.

Appendix C: Transformation of Scannerless Laser Radar Coordinates to Rectangular (x,y,z) Coordinates

Many image processing applications prefer to work with three-dimensional images described in a rectangular (x,y,z) coordinate system. The scannerless laser radar, however, produces images in a pseudo-spherical coordinate system. That is, the range to each pixel in the scene is measured, not its z coordinate in an (x,y,z) coordinate system. (The range to each point is $R=\sqrt{x^2+y^2+z^2}$.) The result is that flat objects will appear curved when viewed in the native laser radar coordinate system. The following is a description of the transformation from the laser radar coordinate system to a rectangular coordinate system.

A standard spherical coordinate system is illustrated in Figure C1. A point in space P which has Cartesian coordinates (x,y,z) will have spherical coordinates (R,θ,ϕ) given by:

$$\phi=\arccos\left[\frac{z}{\sqrt{x^2+y^2+z^2}}\right] \tag{C1}$$

$$\theta=\arctan\left(\frac{y}{x}\right) \tag{C2}$$

$$R=\sqrt{x^2+y^2+z^2} \tag{C3}$$

where R is the distance from the origin O to the point P, ϕ is the angle between the z axis and the line segment OP, and θ is the angle between the x axis and the projection of P onto the x-y plane.

The transformation from spherical coordinates to Cartesian coordinates is given by:

$$x=R\cos(\theta)\sin(\phi) \tag{C4}$$

$$y=R\sin(\theta)\sin(\phi) \tag{C5}$$

$$z=R\cos(\phi) \tag{C6}$$

In the scannerless laser radar, a lens is used to image object points onto a photosensitive array detector (the photocathode of an image intensifier).
For convenience, let's position the origin of the Cartesian coordinate system at the lens of the imaging laser radar as shown in Figure C2. The point P will be imaged onto the photocathode of the laser radar system. If we trace the optical ray that goes through the center of the lens, the angles θ and ϕ will remain the same for the image as those of the object. The z coordinate of the image point is fixed at $z=f$ for

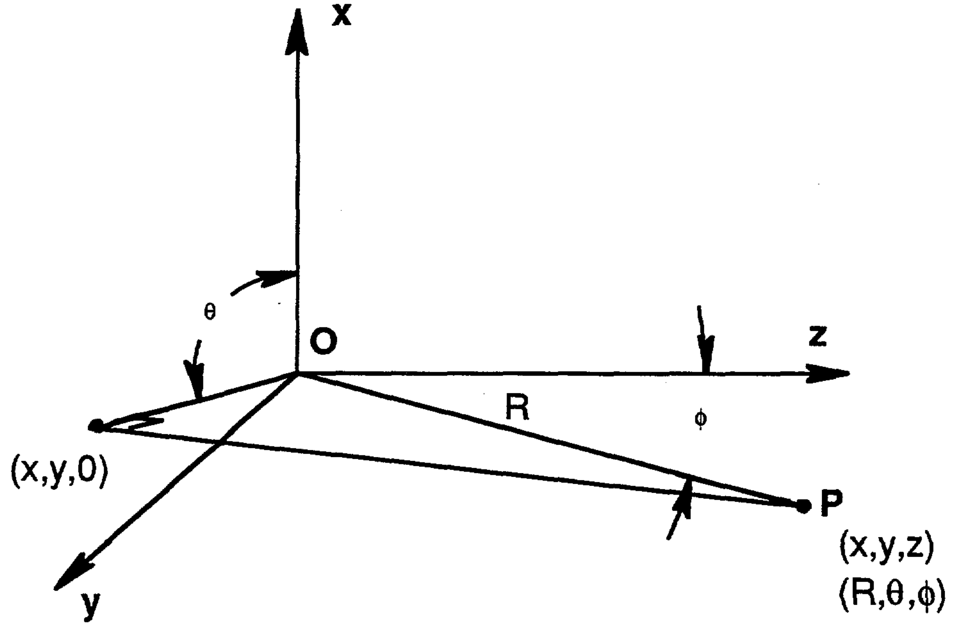

Figure C1. Standard spherical coordinate system. R is the distance from the origin O to the point P, ϕ is the angle between the z axis and the line segment OP, and θ is the angle between the x axis and the projection of P onto the x-y plane.

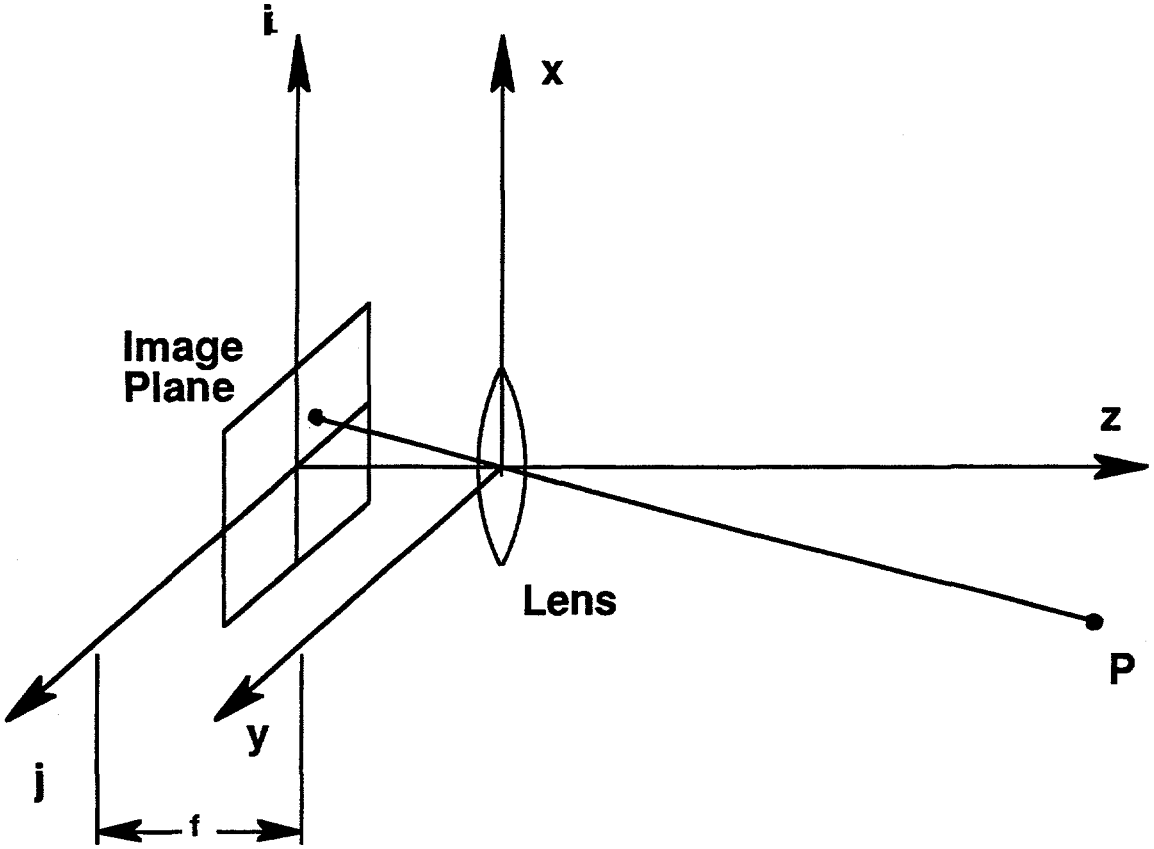

Figure C2. Diagram of the ladar receiver coordinate system. The lens of the ladar system images the point P onto a photosensitive array detector a distance f from the lens. The ladar system uses a pseudo-spherical (i,j,R) coordinate system.

all object points where f is the focal length of the lens. This follows from the fact that the image plane is located one focal length from the lens. Let's call the native coordinate system for the scannerless laser radar system an (i, j, R) coordinate system where

i is the horizontal coordinate of the pixel in the image plane
j is the vertical coordinate in of the pixel in the image plane
R is the range to the scene pixel

The units of i and j are those of the image plane (the photocathode of the image intensifier tube in our case). Thus, if each pixel in the CCD is spaced 16 µm apart and a 3:1 fiber optic taper is used to couple the CCD to the image intensifier tube, each (i, j) increment is 48 µm.

The transformation of the (i, j, R) coordinate system to a spherical coordinate (R, θ, ϕ) coordinate system is:

$$R = R \tag{C7}$$

$$i = f \tan(\phi)\cos(\theta) \tag{C8}$$

$$j = f \tan(\phi)\sin(\theta) \tag{C9}$$

$$\phi = \arccos\left[\frac{f}{\sqrt{i^2 + j^2 + f^2}}\right] \tag{C10}$$

$$\theta = \arctan\left(\frac{j}{i}\right) \tag{C11}$$

where f is the focal length of the lens used to image the scene onto the photocathode of the image intensifier tube.

The transformation from scannerless laser radar coordinates (i,j,R) to rectangular coordinates (x,y,z) is given by:

$$x = R\cos\left(\arctan\left[\frac{j}{i}\right]\right)\sin\left(\arccos\left[\frac{f}{\sqrt{i^2 + j^2 + f^2}}\right]\right) \tag{C12}$$

$$y = R\sin\left(\arctan\left[\frac{j}{i}\right]\right)\sin\left(\arccos\left[\frac{f}{\sqrt{i^2 + j^2 + f^2}}\right]\right) \tag{C13}$$

$$z = R\left(\frac{f}{\sqrt{i^2 + j^2 + f^2}}\right) \tag{C14}$$

Finally, the transformation from rectangular coordinates (x,y,z) to scannerless laser radar coordinates (i,j,R) is given by:

$$R = \sqrt{x^2 + y^2 + z^2} \tag{C15}$$

$$i = f \tan\left\{\arccos\left(\frac{z}{\sqrt{x^2 + y^2 + z^2}}\right)\right\}\cos\left\{\arctan\left(\frac{y}{x}\right)\right\} \tag{C16}$$

$$j = f \tan\left\{\arccos\left(\frac{z}{\sqrt{x^2 + y^2 + z^2}}\right)\right\}\sin\left\{\arctan\left(\frac{y}{x}\right)\right\} \tag{C17}$$

Distribution:

2 Don Holtz
Perceptron, Inc.
23855 Research Drive
Farmington Hills, MI 84335-2643

1 Prof. Dongming Zhao
University of Michigan-Dearborn
Department of Electrical and Computer Engineering
Dearborn, MI 48128-1491

	MS	Name, Org.
20	1423	R. L. Schmitt, 1128
20	0525	T. A. Fischer, 1235
20	0525	R. J. Williams, 1235
1	0311	J. D. Matthews, 2671
1	0525	G. E. Samlin, 1235
1	1425	M. W. Scott, 1307
1	0523	C. F. Gibbon, 1204
1	1423	G. N. Hays, 1128
1	0859	J. T. Sackos, 2527
1	0780	T. H. Cooley, 5838
1	0780	S. Ortiz, 5838
1	0575	R. W. Moya, 5908
1	0780	D. S. Fitzgerald, 5838
1	0859	S. M. Gutierrez, 2527
1	0815	M. R. Muguira, 5933
1	0877	J. P. Anthes, 5932
1	0877	P. Garcia, 5933
1	1423	R. Neal, 1128
1	9051	P. H. Paul, 8351
1	1380	D. J. Lambert, 4213
1	9018	Central Tech Files, 8523-2
5	0899	Technical Library, 4414
2	0619	Review and Approval Desk, 12630 for DOE/OSTI